RADIATION IMPEDANCE OF CAPACITIVE MICROMACHINED ULTRASONIC TRANSDUCERS

A DISSERTATION SUBMITTED TO
THE DEPARTMENT OF ELECTRICAL AND ELECTRONICS ENGINEERING
AND THE INSTITUTE OF ENGINEERING AND SCIENCE
OF BILKENT UNIVERSITY
IN PARTIAL FULFILLMENT OF THE REQUIREMENTS
FOR THE DEGREE OF
DOCTOR OF PHILOSOPHY

By
Muhammed N. Şenlik
January 29, 2010

I certify that I have read this thesis and that in my opinion it is fully adequate, in scope and in quality, as a dissertation for the degree of doctor of philosophy.

Prof. Dr. Abdullah Atalar (Supervisor)

I certify that I have read this thesis and that in my opinion it is fully adequate, in scope and in quality, as a dissertation for the degree of doctor of philosophy.

Prof. Dr. Hayrettin Köymen

I certify that I have read this thesis and that in my opinion it is fully adequate, in scope and in quality, as a dissertation for the degree of doctor of philosophy.

Prof. Dr. Orhan Aytür

I certify that I have read this thesis and that in my opinion it is fully adequate, in scope and in quality, as a dissertation for the degree of doctor of philosophy.

Prof. Dr. Cemal Yalabık

I certify that I have read this thesis and that in my opinion it is fully adequate, in scope and in quality, as a dissertation for the degree of doctor of philosophy.

Assist. Prof. Dr. Ayhan Bozkurt

Approved for the Institute of Engineering and Science:

Prof. Dr. Mehmet Baray
Director of Institute of Engineering and Science

in loving memory of my mother

ABSTRACT

RADIATION IMPEDANCE OF CAPACITIVE MICROMACHINED ULTRASONIC TRANSDUCERS

Muhammed N. Şenlik
Ph.D. in Electrical and Electronics Engineering
Supervisor: Prof. Dr. Abdullah Atalar
January 29, 2010

Capacitive micromachined ultrasonic transducers (cMUTs) are used to transmit and receive ultrasonic signals. The device is constructed from circular membranes fabricated with surface micromachining technology. They have wider bandwidth with lower transmit power and lower receive sensitivity compared to the piezoelectric transducers, which dominate the ultrasonic transducer market. In order to be commercialized, they must overcome these drawbacks or find new application areas, where piezoelectric transducers perform poorly or cannot work. In this thesis, the latter approach, finding a new application area, is followed to design wide band and highly efficient airborne transducers with high output power by maximizing the radiation resistance of the transducer.

The radiation impedance describes the interaction of the transducer with the surrounding medium. The real part, radiation resistance, is a measure of the amount of the power radiated to the medium; whereas the imaginary part, radiation reactance, shows the wobbled medium near the transducer surface. The radiation impedance of cMUTs are currently not well-known. As a first step, the radiation impedance of a cMUT with a circular membrane is calculated analytically using its velocity profile up to its parallel resonance frequency for both the immersion and the airborne applications. The results are verified by finite element simulations. The work is extended to calculate the radiation impedance of an array of cMUT cells positioned in a hexagonal pattern. The radiation impedance is determined to be a strong function of the cell spacing. It is shown that excitation of nonsymmetric modes is possible in immersion applications.

A higher radiation resistance improves the bandwidth as well as the efficiency and the transmit power of the cMUT. It is shown that a center-to-center cell spacing of 1.25 wavelength maximizes the radiation resistance for the most compact arrangement, if the membranes are not too thin. For the airborne applications, the bandwidth can be further increased by using smaller device dimensions, which

decreases the impedance mismatch between the cMUT and the air. On the other hand, this choice leads to degradation in both efficiency and transmit power due to lowered radiation resistance. It is shown that by properly choosing the arrangement of the thin membranes within an array, it is possible to optimize the radiation resistance. To make a fair analysis, same size arrays are compared. The operating frequency and the collapse voltage of the devices are kept constant. The improvement in the bandwidth and the transmit power can be as high as three and one and a half times, respectively. This method may also improve the noise figure when cMUTs are used as receivers. A further improvement in the noise figure is possible when the cells are clustered and connected to separate receivers. The results are presented as normalized graphs to be used for arbitrary device dimensions and material properties.

Keywords: Capacitive Micromachined Ultrasonic Transducer (cMUT), Analytical Modeling, Finite Element Method (FEM) Modeling, Radiation Impedance, Airborne cMUT.

ÖZET

KAPASİTİF MİKROİŞLENMİŞ ULTRASONİK ÇEVİRİCİLERİN RADYASYON EMPEDANSI

Muhammed N. Şenlik
Elektrik ve Elektronik Mühendisliği, Doktora
Tez Yöneticisi: Prof. Dr. Abdullah Atalar
29 Ocak 2010

Kapasitif mikroişlenmiş ultrasonik çeviriciler (cMUT) ultrasonik sinyallerin yayımında ve alımında kullanılmaktadırlar. Cihaz, yüzey mikroişleme teknolojisi ile üretilmiş dairesel zarlardan imal edilmiştir. Ultrasonik çevirici pazarını domine eden piezoelektrik çeviriciler ile karşılaştırıldıklarında daha geniş bant genişliğine sahip olmakla birlikte daha düşük yayım gücü ile daha düşük alım hassasiyetine sahiptirler. Ticarileştirilebilmeleri için bu eksikliklerinin giderilmesi ya da piezoelektrik çeviricilerin kötü çalıştığı veya çalışamadığı alanlarda uygulamalar bulmaları gerekmektedir. Bu tezde, bu yollardan ikincisi, çeviricinin radyasyon rezistansını en yüksek hale getirerek geniş bantlı, yüksek verimli ve yüksek yayım gücüne sahip havada çalışan cMUT'ların tasarımı amacıyla izlenmiştir.

Radyasyon empedansı çeviricinin çevresindeki ortam ile olan etkileşimini tanımlamaktadır. Gerçek kısmı, radyasyon rezistansı, ortama yayımlanan gücün bir ölçüsü iken sanal kısmı, radyasyon reaktansı, çevirici yüzeyinde çalkalanan ortamı göstermektedir. Şu anda cMUT'ların radyasyon empedansı iyi bir şekilde bilinmemektedir. İlk adım olarak, dairesel zara sahip cMUT'ların hız profilleri kullanılarak paralel rezonans frekansına kadarki radyasyon empedansları su ve hava uygulamaları için hesaplanmıştır. Sonuçlar sonlu eleman simülasyonları ile doğrulanmıştır. Çalışma altıgen bir yapı oluşturacak şekilde hücrelerden meydana gelen bir dizinin radyasyon empedansını hesaplamak için genişletilmiştir. Radyasyon empedansının hücreler arasındaki mesafenin kuvvetli bir fonksiyonu olduğu bulunmuştur. Su uygulamalarında simetrik olmayan modların uyarılmasının mümkün olduğu gösterilmiştir.

Daha yüksek bir radyasyon rezistansı bant genişliğiyle birlikte verimi ve yayım gücünü arttırmaktadır. En yoğun yerleşim düzeninde, hücreler arasındaki mesafe dalgaboyunun 1.25 katı olduğu zaman radyasyon rezistansı ince zarlar

için en yüksek değerine ulaşmaktadır. Hava uygulamaları için, cihaz boyutları küçültülerek cMUT ve hava arasındaki empedans uyumsuzluğu azaltılıp bant genişliği arttırılabilmektedir. Öbür yandan, bu seçim radyasyon rezistansının değerini azaltması nedeniyle verimi ve yayım gücünü düşürmektedir. İnce zara sahip cMUT'ların dizi içerisindeki yerleşimi düzenlenerek radyasyon rezistansının en iyileştirilebileceği gösterilmiştir. Adil bir analiz yapabilmek için, aynı alana sahip diziler karşılaştırılmıştır. Cihazların çalışma frekansları ve çökme voltajları sabit tutulmuştur. Bant genişliği ve yayım gücündeki iyileşme üç ve bir buçuk kat daha yüksek olabilmektedir. Bu metod cMUT'lar almaç olarak kullanıldıklarında da gürültü performanslarını iyileştirmektedir. Gürültü performansı, hücreler kümelendirilip farklı almaçlara bağlandığında daha da arttırılabilmektedir. Sonuçlar herhangi bir cihaz boyutu ve malzeme özelliği için kullanılabilmeleri amacıyla normalize grafikler halinde sunulmuştur.

Anahtar sözcükler: Kapasitif Mikroişlenmiş Ultrasonik Çevirici (cMUT), Analitik Modelleme, Sonlu Eleman Metodu (SEM) ile Modelleme, Radyasyon Empedansı, Havada Çalışan cMUT.

ACKNOWLEDGEMENTS

I would like to express my sincere gratitude to Prof. Atalar for his supervision, guidance and encouragement through the development of this thesis. He was the perfect supervisor for me.

I would like to thank to the members of my thesis jury for reading the manuscript and commenting on the thesis.

Selim and Elif, there are no words to describe them or no ways to thank them.

Endless thanks to Emre Kopanoğlu and Onur Bakır for their supports. I must also thank to my labmates, Burak, Ceyhun, Deniz, Kağan and Vahdet, who have to see my Gargamel face everyday.

Many thanks to my friends, students and professors, whose names I forgot to mention. Some times, a little smile makes my day.

Without my family, this work would be never be possible.

Finally, my brother, Servet. Although I am the elder one, he was both a father and a mother for me. Thanks for always being there.

Contents

List of Figures

List of Tables

Chapter 1

INTRODUCTION

Capacitive micromachined ultrasonic transducers (cMUTs) were first reported in [1, 2]. The device is simply a parallel plate capacitor with one moving electrode fabricated with surface micromachining technology [3–6] as seen in Fig. 1.1. They are used in the areas of medical imaging [7–10], underwater acoustics [11], audio range sound generation [12] and detection [13, 14], non-destructive evaluation of solids [15,16], micro fluidic applications [17,18], Lamb [19] and Scholte [20] waves generation and detection, atomic force microscopy [21, 22], chemical sensors [23] and parametric amplification [24].

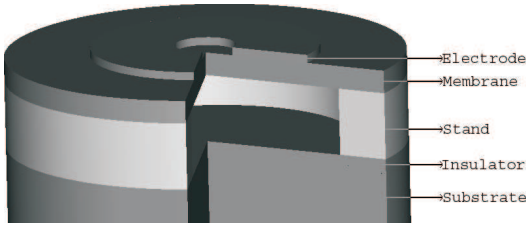

Figure 1.1: 3D view of a cMUT cell.

There are two major methods for the fabrication of cMUTs. In the conventional method [3, 5, 6], a sacrificial layer is used to define the gap and the membrane is grown on top of it. Later, the sacrificial layer is etched with the aid of the etch holes. In the wafer bonding method [4, 6], two separate wafers are used for the ground and the membrane. Depending on the process, the gap is

defined on one of the wafers. Then, these wafers are bonded with a wafer bonder. It is possible to fabricate cMUTs using a foundry [25–27], however this process lacks the sealing of the membranes. Also, each research group developed their fabrication processes based on these methods.

Compatibility with silicon IC technology and ease of construction of arrays made cMUTs an alternative to piezoelectric tranducers, which are currently used in most of the applications mentioned above. cMUTs offer wider bandwidth [28, 29], however, they provide approximately 10-dB lower loop gain [28, 29] [1] compared to their alternatives which is one of the reasons not to be commercialized. There are various techniques to increase the loop gain of cMUTs. These are changing the membrane structure [30–35], operating in different regimes [36], use of different detection techniques [23, 37, 38] and use of different electrical circuitry [39, 40]. However, each method brings disadvantages, such as high operating voltages or an extra detection structure, which may not be silicon compatible.

1.1 Analysis

1.1.1 Modeling

The modeling is an important tool to characterize and design transducers. There are two approaches followed in the modeling of cMUTs, analytical modeling and modeling with finite element method (FEM) simulations. The former one starts with the solution of the differential equation governing the membrane motion [2, 41]. Then, an equivalent circuit known as Mason's equivalent circuit is constructed. The parameters of these equivalent circuit is obtained from the above solution together with the actual device dimensions. In [42, 43], the transformers ratio of cMUT is calculated and in [1, 2, 44, 45], the mechanical impedance

[1] The loop gain is defined as the ratio of the received voltage to the applied voltage in pulse-echo mode.

of the membrane is replaced with a series LC section. Yaralioglu *et al.* [46], Ronnekleiv [47] and Senlik *et al.* [48] calculated the radiation impedance of the membrane. In the latter approach, the complete model of cMUT is implemented with a commercially available software package [49–51] or a cMUT specific tool [52]. Also it is possible to implement the equations governing cMUT operation with a circuit analysis tool [53, 54] to construct an equivalent circuit.

In this thesis, the analytical approach followed in [48, 55] is used with the simplifying assumptions. The FEM simulations are used only for the verification purposes.

1.1.2 Radiation Impedance

The radiation impedance describes the interaction of the transducer with the surrounding medium. The real part, the radiation resistance, denotes the quantitative amount of the power radiated to the medium; whereas the imaginary part, the radiation reactance, shows the quantitative stored energy in the near field. The radiation impedance of cMUTs are currently not well-known. In this thesis, the radiation impedance of cMUTs with circular membranes is calculated.

The mechanical impedance of a cMUT membrane in vacuum is well studied [45]. It shows successive series and parallel resonances, where force and velocity becomes zero, respectively [56]. When a cMUT is immersed in water, the acoustic loading on the cell is high and results in a wide bandwidth. All mechanical resonance frequencies shift to lower values because of the imaginary part of the radiation impedance. If a cMUT is used in air, the radiation impedance is rather low and the bandwidth is limited by the mechanical Q of the membrane. It is therefore preferable to increase the radiation resistance in order to get a higher bandwidth in airborne applications. Moreover, for the same membrane motion, a higher acoustic power is delivered to the medium, if the radiation resistance is higher. Hence, a higher radiation resistance is desirable to be able to transmit more power, since the gap limits the maximum allowable membrane motion.

The efficiency of a transducer is defined as the ratio of the power radiated to the medium to the power input to the transducer [57]. The loss in a cMUT due

to the electrical resistive effects and the mechanical power lost to the substrate can be represented as a series resistance [1]. Hence, the efficiency will increase if the radiation resistance increases in both airborne and immersion cMUTs, since a smaller portion of the energy will be dissipated on the loss mechanisms such as the coupling into the substrate.

There are several approaches to model the radiation impedance of the cMUT membrane. In [46], the radiation impedance is modelled using an equal size piston radiator. In [58], an equivalent piston radiator with the appropriate boundary conditions is defined and its radiation impedance is used. In [59, 60], the radiation impedance of an array is modelled with lumped circuit elements. In [61], the radiation impedance is calculated by subtracting the mechanical impedance of the membrane from the input mechanical impedance as computed by a finite element simulation. In [47], cMUT is modelled with a modal expansion based method and the radiation impedance is calculated using that method. Caronti *et al.* [62] calculated the radiation impedance of an array of cells performing finite element method simulations with a focus on the acoustic coupling between the cells.

1.2 Applications

Airborne ultrasound has many applications in diverse areas, generally requiring high bandwidth. The impedance mismatch between air and the transducer causes a reduction of bandwidth of the device. cMUTs offer wider bandwidth in air compared to the piezoelectric counterparts at the expense of lower transmit power and receive sensitivity. In this thesis, the bandwidth of cMUT operating in air is optimized without degrading the transmit and the receive performance.

cMUTs used in air require membranes with high radius-to-thickness ratios and high gap heights due to the frequency requirements and the effect of the atmospheric pressure. The conventional fabrication of cMUTs, the sacrificial layer method [3, 5] does not allow the fabrication of these large membranes [4, 6]. The use of the wafer bonding technology [4] and the optimization of the process make possible the production of the reliable cMUTs operating in air.

There are various methods to increase the bandwidth of cMUTs. Using thinner membranes decreases the membrane impedance and hence reduces the quality factor [63]. Introducing lossy elements to the electrical terminals of the device may also work at the expense of reduced efficiency and sensitivity. On the other hand, increasing the radiation resistance also helps without causing a reduction in the efficiency [48, 64] as mentioned previously.

Chapter 2 gives the fundamentals and the basic operation principles of cMUT. This chapter also includes the modelling used throughout this thesis. Chapter 3 presents the calculation of the radiation impedance of cMUT by analytical means. Chapter 4 describes the application of the model to design wide band, highly efficient airborne cMUTs with high output power. The last chapter concludes this thesis.

Chapter 2

FUNDAMENTALS of cMUT

In this chapter, capacitive micromachined ultrasonic transducers (cMUTs) are introduced and a complete model of cMUT used in this thesis is presented. First, a single cMUT cell and its static behavior are described. Then, the analytical and the finite element models of cMUTs are constructed with the simplifying assumptions.

2.1 cMUTs

Fig. 2.1(a) shows the cross-section of a single cMUT cell fabricated with a low temperature fabrication process [5]. The whole structure lies on a silicon substrate. A patterned metal layer forms the bottom electrode. There is a thin layer of silicon nitride above the bottom electrode. Vibrating silicon nitride membrane is supported by silicon nitride anchors. Another patterned metal layer forms the top electrode. The gap that is formed inside the structure is sealed. cMUTs are used in array configuration. Fig. 2.1(b) shows a close view of a fabricated array.

When a voltage is applied between the electrodes, the membrane deflects towards the substrate due to the electrostatic forces. As the voltage is increased, the slope of the voltage-deflection curve increases. At the collapse voltage, V_{col}, the restoring forces of the membrane cannot resist the electrostatic forces and

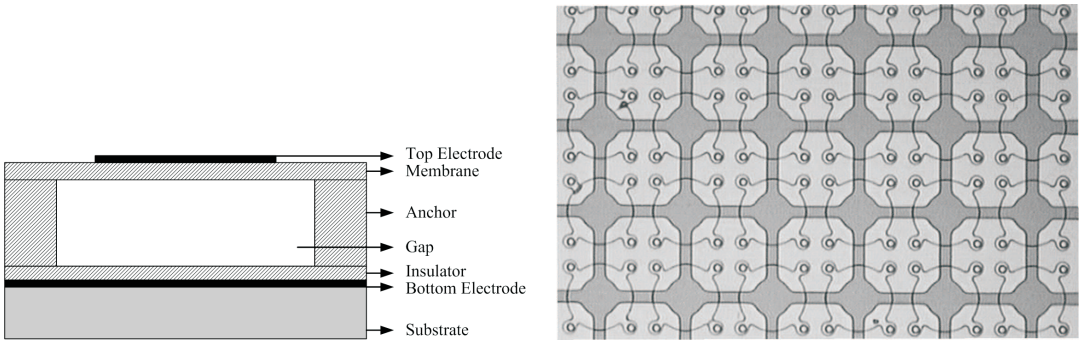

(a) (b)

Figure 2.1: (a) Cross-section of a single cMUT cell fabricated with a low temperature fabrication process. (b) Close view of a fabricated array. The light and the dark gray regions show the membrane and the electrode. Fig. 2.1(a) is the cross section of this region.

membrane collapses onto the insulator [2, 65]. Until the voltage is decreased to snap-back voltage, V_{sb}, the membrane contacts with the insulator and then snaps back [2, 65]. The hysteresis behavior and the membrane shapes for various voltages are shown in Fig. 2.2 [36].

During transmit, cMUT is driven with a high amplitude pulse. In the reception, it is biased close to V_{col} and change in current caused by a sound wave hitting the membrane is measured. Fig. 2.3 shows typical transmit and receive circuits. There are two operating regimes for cMUTs. In conventional regime [2], cMUT is operated such that it does not collapse. In collapse regime [36], cMUT is operated while the membrane is in contact with the substrate.

2.2 Modeling

The geometry of a cMUT cell is illustrated in Fig. 2.4 to establish the notation. Here, a and t_m are the radius and the thickness of the membrane, respectively. t_g is the distance of the gap underneath the membrane. Y_0, ρ, ν and T are the Young's modulus, the density, the Poisson's ratio and the residual stress of the membrane material, respectively. The membrane area, πa^2 is denoted by S. The material properties used in the simulations can be found in Table 2.1.

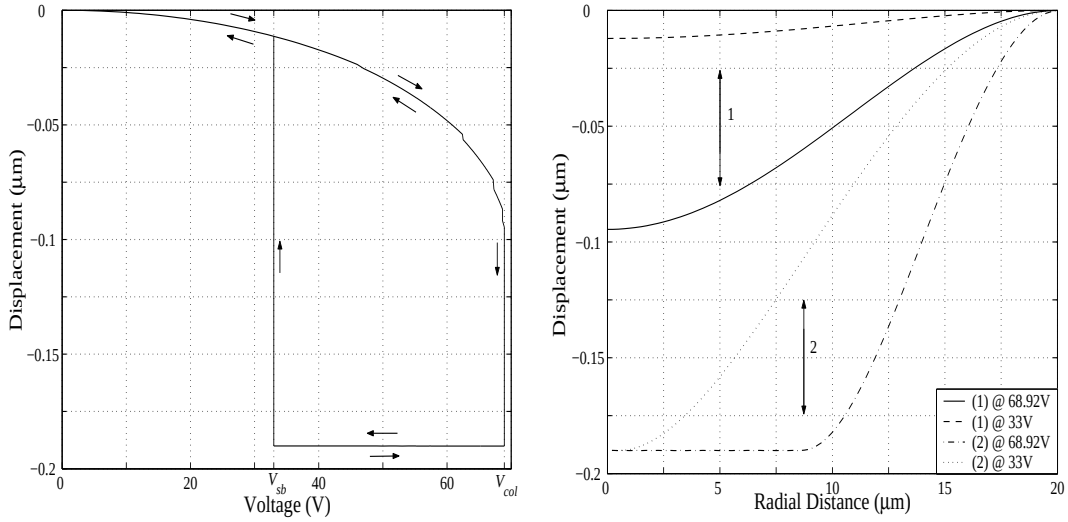

(a) (b)

Figure 2.2: (a) Deflection of the center of the membrane with respect to the applied voltage. Arrows indicate the direction of the movement as the voltage is changed. (b) Membrane shapes for various voltages just around collapse and snap-back. Region 1 and 2 are before and during collapse, respectively. The radius and the thickness of the membrane and the gap height are 20 μm, 1 μm and 0.2 μm, respectively. The membrane material is Si_3N_4.

2.2.1 Analytical Modeling

cMUT is a distributed structure, however in order to model by analytical means; scalar quantities are used to define cMUT behavior with a single simplifying assumption. It is assumed that as the membrane moves, the surface profile does not change. Note that it is also possible to approximate the membrane shape as shown in [45] for a more accurate model.

Mechanical Impedance of cMUT Membrane

The mechanical impedance of cMUT referred to the average velocity is defined as the ratio of the total force (assuming uniform pressure [1]) applied to the membrane

[1]Note that when the membrane is under bias, the uniform pressure assumption isn't correct. In that case, a FEM simulation must be performed for the exact answer [45].

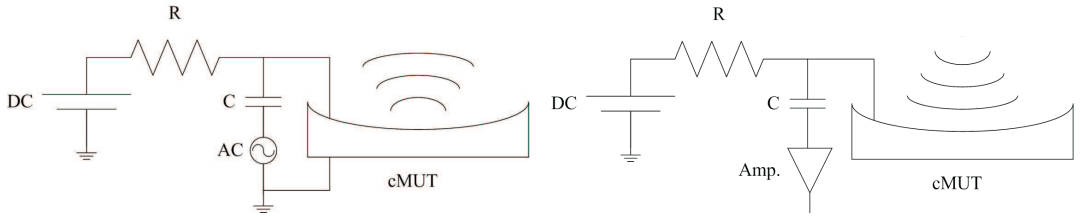

Figure 2.3: cMUT used in (a) transmit and (b) receive configurations. In both configurations, cMUT is DC biased with a source and a resistor. During the transmission, a pulse is applied over a capacitor and during the reception an amplifier is connected through a capacitor.

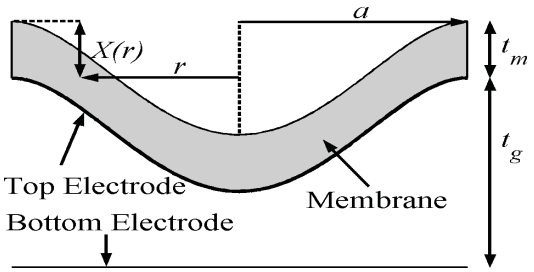

Figure 2.4: Geometry of a cMUT cell under deflection.

to the resulting average velocity [2, 41]

$$Z_m = \frac{F}{V_{ave}} = j\omega\pi a^2 t_m \rho \left[\frac{ak_1k_2(k_1J_0(k_2a)J_1(k_1a) - k_2J_0(k_1a)J_1(k_2a))}{ak_1k_2(k_1J_0(k_2a)J_1(k_1a) - k_2J_0(k_1a)J_1(k_2a)) - 2(k_1^2 - k_2^2)J_1(k_1a)J_1(k_2a)} \right] \tag{2.1}$$

where ω is the radial frequency and J_0 and J_1 are the zeroth and the first order Bessel functions of the 1st kind with

$$c = \frac{(Y_0 + T)t_m^2}{12(1-\nu^2)\rho}, \quad d = \frac{T}{\rho} \tag{2.2}$$

and

$$k_1 = \sqrt{\frac{-d + \sqrt{d^2 + 4c\omega^2}}{2c}}, \quad k_2 = j\sqrt{\frac{d + \sqrt{d^2 + 4c\omega^2}}{2c}} \tag{2.3}$$

The mechanical impedance of cMUT (2.1) shows successive series and parallel resonances in vacuum as depicted in Fig. 2.5. The first series resonance frequency, f_r, is at 12 MHz, whereas the first parallel resonance frequency, f_p, is at 41 MHz for the particular membrane.

Table 2.1: Material parameters used in the simulations.

Parameter	Si_3N_4	Si	Water	Air
Y_0, Young's modulus (GPa)	320	169		
ν, Poisson's ratio	0.263	0.27		
ρ, Density (kg/m^3)	3270	2332	1000	1.27
c_0, Speed of sound (m/s)			1500	331

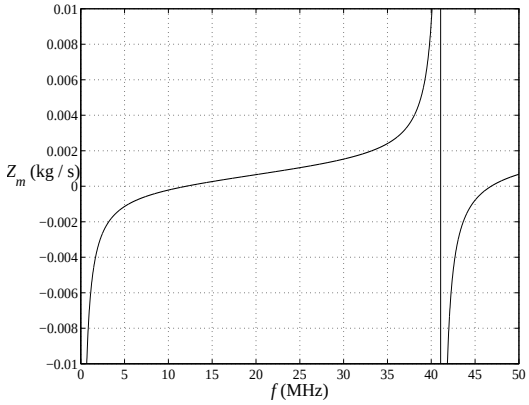

Figure 2.5: Mechanical impedance of cMUT in vacuum. a=20 μm and t_m=1 μm. The membrane material is Si_3N_4 and T=0 Pa.

Mason's Equivalent Circuit

cMUT typically operates below its parallel resonance frequency [1]. Hence, the following model is constructed for the frequencies less than f_p, valid up to $0.4f_p$. rms displacement is chosen rather than average displacement as the reference. Initially, the effects of the spring softening [46], the stress stiffening [66] and the deflection under an external force [55] are ignored. The displacement phasor, X, of the cMUT membrane is dependent on the radial position, r, and can be approximated up to $0.4f_p$ by the equation [48, 55]

$$X(r) = \sqrt{5}x_{rms}\left(1 - \frac{r^2}{a^2}\right)^2 U(a-r) \tag{2.4}$$

where U is the unit step function and x_{rms} denotes the rms displacement phasor over the surface of the membrane [48] [2]. Undeflected and deflected capacitances

[2] As shown in Chapter 3, it is possible to write the displacement profile of the cMUT membrane as a superposition of the parabolic displacement profiles. Then, using superposition, it is possible to extend the modeling up to f_p.

of cMUT and its derivative with respect to x_{rms} are given by [55]

$$\begin{aligned} C_0 &= \frac{\epsilon_0 \pi a^2}{t_g} \\ C &= C_0 \frac{\tanh^{-1}\left(\sqrt{\sqrt{5}x_{rms}/t_g}\right)}{\sqrt{\sqrt{5}x_{rms}/t_g}} \\ \frac{\mathrm{d}C}{\mathrm{d}x_{rms}} &= \frac{C_0}{2x_{rms}\left(1-\sqrt{5}x_{rms}/t_g\right)} - \frac{C}{2x_{rms}} \end{aligned} \tag{2.5}$$

where ϵ_0 is the free space permittivity. The top electrode is assumed to be under the membrane surface, equivalently the membrane material is conductive. Assuming no nonlinearity and no initial deflection under an external force, V_{col} of the membrane is given by the expression [55]

$$V_{col} = 0.39\sqrt{\frac{16 Y_0 t_m^3 t_g^3}{(1-\nu^2)\epsilon_0 a^4}}. \tag{2.6}$$

If the operating voltage, V_{DC}, is equal to αV_{col}, then the turns ratio, n, in the Mason's equivalent circuit [1, 41], Fig. 2.6 is [55]

$$n = V_{DC}\frac{\mathrm{d}C}{\mathrm{d}x_{rms}}. \tag{2.7}$$

The mechanical impedance of the membrane up to $0.4f_p$ can be modelled with a series LC section, whose values are found by [45, 55]

$$\begin{aligned} L_m &= \pi a^2 t_m \rho \\ C_m &= \frac{(1-\nu^2)a^2}{8.9\pi Y_0 t_m^3}. \end{aligned} \tag{2.8}$$

Hence, the series resonance frequency is found as

$$f_r = \frac{1}{2\pi\sqrt{L_m C_m}} = \frac{0.47 t_m}{a^2}\sqrt{\frac{Y_0}{\rho(1-\nu^2)}} \tag{2.9}$$

and the wavelength at f_r, λ_r, is

$$\lambda_r = \frac{c_0}{f_r} = \frac{2.1 a^2 c_0}{t_m}\sqrt{\frac{\rho(1-\nu^2)}{Y_0}} \tag{2.10}$$

where c_0 is the speed of sound in the medium. The radiation impedance of the cMUT cell is written as [48]

$$Z_r = R_r + iX_r = S\rho_0 c_0(R_n + iX_n) \tag{2.11}$$

where ρ_0 is the density of the medium. R_n and X_n are the normalized radiation resistance and reactance.

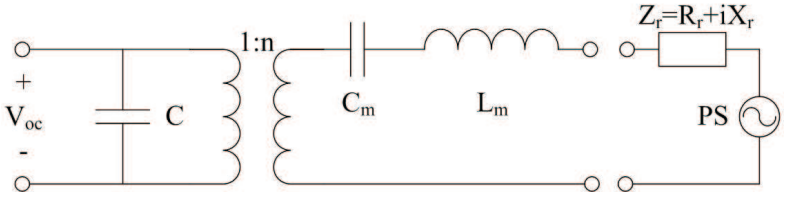

Figure 2.6: Mason's equivalent circuit of cMUT. C is the shunt input capacitance and n is the turns ratio. The membrane impedance up to $0.4f_p$ is modelled with a series LC section. During the reception, cMUT is excited by a force source with an amplitude of PS, where P is the incident pressure field.

The spring softening can be modeled by connecting a capacitor of value $-C$ at the electrical side in series with the transformer in Mason's equivalent circuit. To calculate the deflection under an external force F_{ext}, like atmospheric pressure, the deflection, x_{ext} can be found by solving [55]

$$F_{ext} = k_1 x_{ext} \tag{2.12}$$

where k_1=$1/C_m$ is the linear spring constant. The spring stiffening can be modeled by using a nonlinear third order spring constant [55]

$$k_3 = \frac{-2\pi Y_0 t_m(-896585 - 529610\nu + 342831\nu^2)}{29645a^2} \tag{2.13}$$

with the total mechanical force

$$F = k_1 x_{rms} + k_3 x_{rms}^3. \tag{2.14}$$

However, in cases when the ratio of the membrane thickness to radius and gap height is high, use of k_3 is not enough and a finite element method simulation must be performed in order to make a correct modeling [66]. Following [67], it is possible to calculate V_{col} when F_{ext} and k_3 are present.

Directivity

The directivity is defined as the ratio of the radiation intensity in a given direction from the tranducer to the radiation intensity averaged over all directions, given as for a single cell [68]

$$D(\theta) = \frac{48 J_3(ka\sin\theta)}{(ka\sin\theta)^3} \tag{2.15}$$

where θ is the polar angle and J_3 is the third order Bessel function. 48 is used for normalization to 1. Fig. 2.7(a) shows the directivity of a single cell with ka=2. The directivity of the array can be found by the superposition of the individual cells. Fig. 2.7(b) shows the directivity of the array in Fig. 3.3.

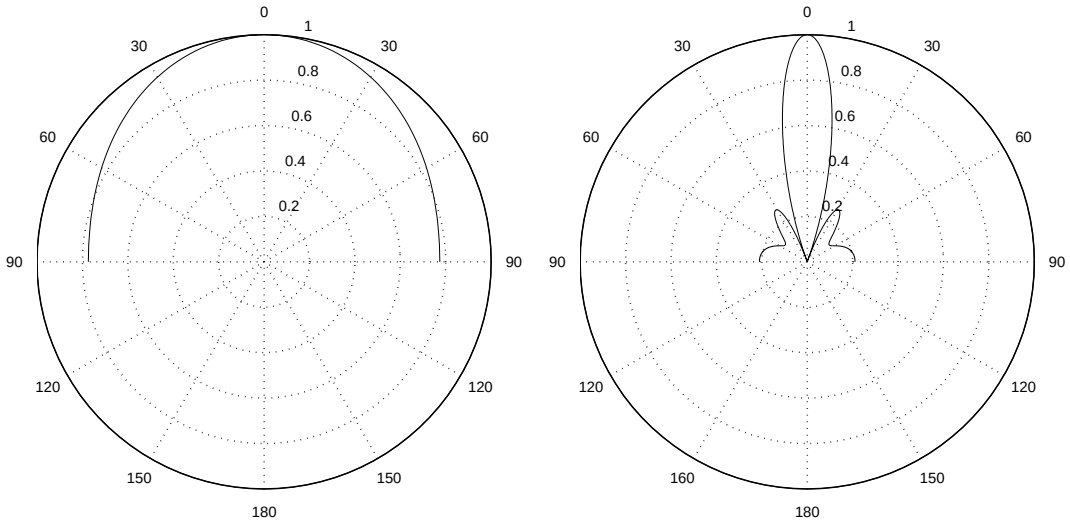

Figure 2.7: Directivity of (a) a single cell (b) array in Fig. 3.3. ka=2 for the cMUT cell.

2.2.2 Finite Element Method (FEM) Modeling

ANSYS (ANSYS Inc., Canonsburg, PA) and COMSOL (COMSOL Inc., Burlington, MA) are used in FEM modeling. 2D axial symmetric models are implemented

using ANSYS [3] to calculate the DC and the AC behaviors with the velocity and the pressure profiles on the surface of the cMUT membrane [49–51]. The circular absorbing boundary is 2λ away from the membrane at the lowest operating frequency and the mesh size is $\lambda/40$ at the highest operating frequency. A rigid baffle is assumed.

3D models are implemented using COMSOL [4]. The absorbing boundary is 0.5λ away from the membrane and the mesh size is $\lambda/5$ at the operating frequency.

[3]The membrane, the fluid and the absorbing boundary are modeled using PLANE42, FLUID29 and FLUID129 elements, respectively. Electrostatic elements are modeled using TRANS126 elements.

[4]acsld and acpr multiphysics environments are used for the structural and the acoustic solutions, respectively. DC and AC analyses are not implemented.

Chapter 3

RADIATION IMPEDANCE

In this chapter, the radiation impedance of an array of cMUT cells with circular membranes is presented. First, the radiation impedance of a single cMUT cell is calculated using its velocity profile. Then, the radiation impedance of array of cMUT cells is calculated from analytical expressions and compared with those found from finite element simulations.

3.1 Mechanical Behavior of a Circular cMUT Membrane

3.1.1 Velocity Profile

The velocity profile on the surface of a circular radiator can be expressed analytically using a linear combination of functions given by [48, 55, 69, 70]

$$v_n(r) = V_{rms}\sqrt{2n+1}\left(1-\frac{r^2}{a^2}\right)^n U(a-r) \tag{3.1}$$

where U is the unit step function. n =0, 1 and 2 correspond to the velocity profiles of rigid piston, simply supported and clamped radiators [1], respectively as

[1]The analytical model of cMUT in Chapter 2 assumes that the cMUT membrane has a displacement, equivalently velocity profile of (3.1) with n=2.

seen in Fig. 3.1(a). V_{rms} denotes the rms velocity over the surface of the radiator given by

$$V_{rms} = \sqrt{\frac{1}{S}\int_S \mathrm{Re}\{v(r)\}^2 dS} + i\sqrt{\frac{1}{S}\int_S \mathrm{Im}\{v(r)\}^2 dS} \tag{3.2}$$

With this definition, V_{rms} is a complex number representing the phasor of the lumped membrane velocity and is non-zero for all velocity profiles.

A radially symmetric velocity profile, $v(r)$, can be written in terms of the velocity profiles of (3.1) as

$$\begin{aligned} v(r) &= \alpha_0 v_0(r) + \alpha_1 v_1(r) + \cdots + \alpha_N v_N(r) \\ &= \sum_{n=0}^{N} \alpha_n v_n(r) \end{aligned} \tag{3.3}$$

The values of the coefficients, α_n, are calculated by first equating V_{rms} in each $v_n(r)$ to V_{rms} of $v(r)$ resulting in

$$\begin{aligned} &\alpha_0^2 + \sqrt{3}\alpha_0\alpha_1 + \cdots = 1 \\ &\sum_{n=0}^{N}\sum_{m=0}^{N} \frac{\sqrt{2n+1}\sqrt{2m+1}}{n+m+1}\alpha_n\alpha_m = 1 \end{aligned} \tag{3.4}$$

and then using the least mean square algorithm with (3.4) to fit the velocity distribution to the actual one.

The velocity profile of a cMUT membrane depends on f/f_p [2]. This profile determined by FEM simulations can be seen in Fig. 3.1(b) for f=0.2f_p and can be approximated using (3.3) with α_2=0.94 and α_4=0.06. The same figure also shows the velocity profiles of the membrane at f=0.4f_p and f=f_p with α_2=0.71, α_4=0.3 and α_2=-2.45, α_4=3.06, respectively, approximating the profiles very accurately. The variation of α_2 and α_4 is given in Table 3.1 as a function of f/f_p.

3.1.2 Radiation Impedance

As mentioned in the previous section, cMUT is a distributed structure. However, in this work, its displacement and velocity profiles are modeled with a lumped

[2]The parallel resonance frequency (f_p) corresponds to the second circularly symmetric mode of the membrane.

Table 3.1: Variation of α_2 and α_4 with respect to f/f_p.

f/f_p	0	0.1	0.2	0.3	0.4	0.5	0.6	0.7	0.8	0.9	1
α_2	1	0.99	0.94	0.85	0.71	0.50	0.20	-0.23	-0.86	-1.64	-2.45
α_4	0	0.012	0.063	0.15	0.30	0.51	0.81	1.22	1.79	2.45	3.06

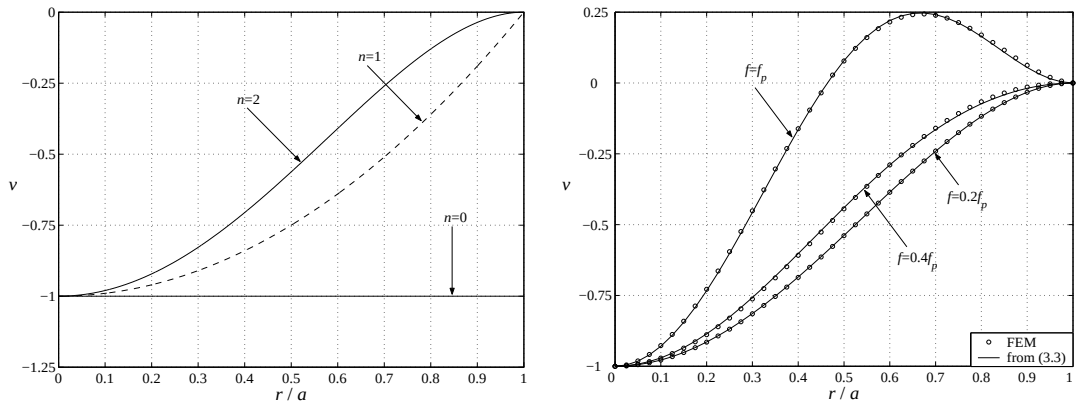

(a) (b)

Figure 3.1: (a) The velocity profiles of rigid piston, simply supported and clamped radiators normalized to the peak values (b) The velocity profiles of a cMUT membrane normalized to the peak values determined by FEM simulations at f=0.2f_p, 0.4f_p and f_p. The same profiles approximated using (3.3) with [α_2=0.94, α_4=0.06], [α_2=0.71, α_4=0.3] and [α_2=-2.45, α_4=3.06] are also shown.

velocity variable, v_{rms}, and a function of the radial distance, r. When the square of this lumped velocity, V, is multiplied with the radiation impedance, Z,

$$P = V^2 Z \tag{3.5}$$

it gives the total power at the surface of cMUT, P. Hence, the radiation impedance, Z, of a transducer with a velocity profile, $v(r)$, can be found by dividing the total power, at the surface of the transducer to the square of the absolute value of an arbitrary reference velocity, V, [71, 72]

$$Z = \frac{P}{|V|^2} = \frac{\int_S p(r) v^*(r) dS}{|V|^2} \tag{3.6}$$

where $p(r)$ and $v^*(r)$ are the pressure and the complex conjugate of velocity at the radial distance r. All of the work on modelling the membranes since Mason [41] employ the average velocity, V=V_{ave}, to represent the reference velocity variable.

This choice is problematic with some higher mode cMUT velocity profiles, since it may give V=0 [45] resulting in an infinite radiation impedance. In this thesis, the reference velocity is chosen to be the root mean square velocity, V=V_{rms} , defined in (3.2). Note that with each choice of the reference velocity, a different radiation impedance will be obtained and the equivalent circuit variables must be calculated based on this reference velocity.

For the velocity profile of (3.3), the total radiated power is

$$\begin{aligned} P &= \int_S \sum_{n=0}^{N} \sum_{m=0}^{N} \alpha_n \alpha_m p_n(r) v_m^*(r) dS \\ &= \sum_{n=0}^{N} \sum_{m=0}^{N} \alpha_n \alpha_m P_{nm} \end{aligned} \tag{3.7}$$

where P_{nm} is the power generated by $v_m(r)$ in the presence of the pressure field, $p_n(r)$ generated by $v_n(r)$. Following [70], P_{nm} can be expressed in a closed form as

$$P_{nm} = S\rho_0 c_0 V_{rms}^2 A \left\{1 - B\left[F_{1nm}(2ka) + iF_{2nm}(2ka)\right]\right\} \tag{3.8}$$

where k is the wavenumber and while A and B are constants, F_{1nm} and F_{2nm} are some functions of ka given in Table 3.2 for n, m=2 and 4. Table 3.3 gives the small argument approximations of $P_{nm}/S\rho_0 c_0 V_{rms}^2$ in (3.8) for $ka < 0.25$ to overcome the numerical accuracy problems during the calculation of Bessel and Struve function terms.

Using (3.3) with n=2 and 4 and combining with (3.6), (3.7) and (3.8), Z is found as

$$Z = R + iX = \frac{\alpha_2^2 P_{22} + 2\alpha_2 \alpha_4 P_{24} + \alpha_4^2 P_{44}}{|V_{rms}|^2} \tag{3.9}$$

Here, R is the real part and X is the imaginary part of the radiation impedance. The real part is due to the real power radiated into the medium, whereas the imaginary part is due to the stored energy in the medium due to the sideways movements of the medium in the close proximity of the membrane.

The radiation impedance computed from (3.9) and normalized by $S\rho_0 c_0$ for piston and clamped radiators (with velociy profiles given by (3.1) for n=0 and n=2) can be seen in Fig.3.2 as a function of ka. As $ka \to \infty$, the mutual effects vanish and the normalized radiation resistance for both radiators converge to unity [68, 73]. For the same case, the radiators do not generate reactive power,

hence the radiation reactances of both radiators approach to zero. The figure also shows the normalized radiation impedances of three cMUT membranes with different $k_p a$ values as computed from (3.9), where k_p is the wavenumber at the parallel resonance frequency. The velocity profiles corresponding to different ka values are calculated from Table 3.1 using $ka/k_p a{=}f/f_p$ ratios. The frequencies less than the parallel resonance frequency of the cMUT membrane ($ka \leq k_p a$) are considered. cMUTs are similar to the clamped radiators for $ka < 0.4 k_p a$. In this range, the velocity profile of the cMUT membrane follows that of the clamped radiator. But, for $ka > 0.4 k_p a$, deviations from the clamped radiator behavior occur, especially when $k_p a$ is small and the mutual effects are significant. On the other hand, if $k_p a$ is high, the mutual effects are insignificant and R approaches to that of the clamped radiator.

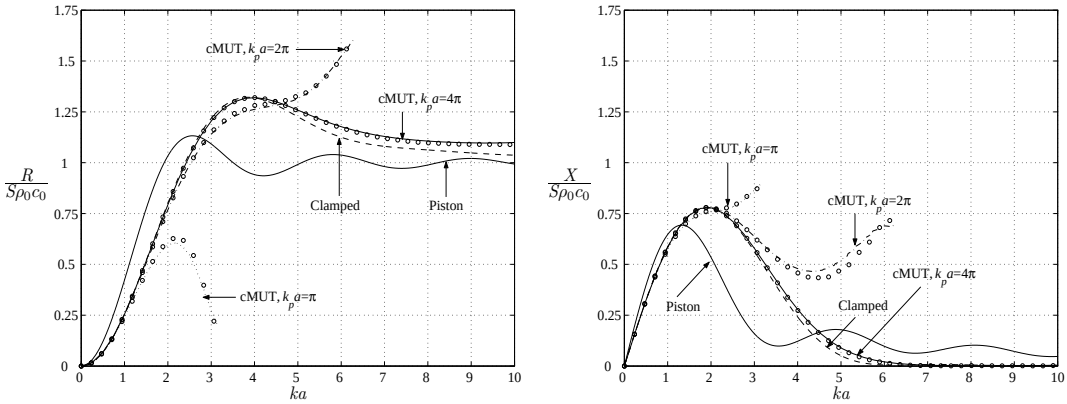

(a) (b)

Figure 3.2: The calculated radiation (a) resistance (b) reactance normalized by $S\rho_0 c_0$ of a piston radiator, a clamped radiator and cMUT membranes with $k_p a{=}\pi$, 2π and 4π. The radiation impedances of the cMUT membranes determined by FEM simulations (circles) are also included. The curves for cMUT membranes are shown for $ka \leq k_p a$.

Table 3.2: Constants and functions used in (3.8).

n	m	A	B	$F_{1nm}(y)$	$F_{2nm}(y)$
2	2	1	$\frac{2^{11}\cdot 5}{(2ka)^7}$	$y^2J_5(y)+2yJ_4(y)+3J_3(y)$	$-y^2H_5(y)-2yH_4(y)-3H_3(y)$
				$-y^3/16-y^5/768$	$+(2/\pi)\cdot(y^4/35)+(2/\pi)\cdot(y^6/945)$
2	4	$\frac{3\sqrt{5}}{7}$	$\frac{2^{17}\cdot 3\cdot 7}{(2ka)^{11}}$	$y^4J_7(y)+5y^3J_6(y)+27y^2J_5(y)$	$-y^4H_7(y)-5y^3H_6(y)-27y^2H_5(y)$
				$+105yJ_4(y)+210J_3(y)-35y^3/8$	$-105yH_4(y)-210H_3(y)+(2/\pi)\cdot(2y^4)$
				$-y^7/(5.12\times10^3)-y^9/(1.84\times10^5)$	$+(2/\pi)\cdot(y^6/27)+(2/\pi)\cdot(2y^8/(3.47\times10^3))$
4	4	1	$\frac{2^{23}\cdot 3^4}{(2ka)^{13}}$	$y^4J_9(y)+4y^3J_8(y)+18y^2J_7(y)$	$-y^4H_9(y)-4y^3H_8(y)-18y^2H_7(y)$
				$+60yJ_6(y)+105J_5(y)-7y^5/256$	$-60yH_6(y)-105H_5(y)+(2/\pi)\cdot(y^6/99)$
				$-y^7/(6.14\times10^3)-y^9/(5.73\times10^5)$	$+(2/\pi)\cdot(5y^8/(2.70\times10^4))+(2/\pi)\cdot(y^{10}/(4.05\times10^5))$
				$-y^{11}/(3.30\times10^7)$	$(2/\pi)\cdot(y^{12}/(3.45\times10^7))$

J_n and H_n are the nth order Bessel and Struve functions.

Table 3.3: Small argument approximations of the real and the imaginary parts of $P_{nm}/S\rho_0 c_0 V_{rms}^2$ in (3.8). (y=ka)

n	m	Real	Imaginary
2	2	$5y^2/72 - 5y^4/(3.46 \times 10^3)$	$2^{15}y/(3.12\pi \times 10^4)$
2	4	$\sqrt{5}y^2/40 - \sqrt{5}y^4/(2.30 \times 10^3)$	$2^{22}\sqrt{5}/(1.01\pi \times 10^7) - 2^{24}\sqrt{5}y^3/(1.47\pi \times 10^9)$
4	4	$9y^2/200 - 9y^4/(1.44 \times 10^4)$	$2^{31}y/(2.55\pi \times 10^9 - 2^{31}y^3/(1.18\pi \times 10^{11}))$

3.2 Radiation Impedance of an Array of cMUT Cells

cMUTs are used in array configuration. To calculate the radiation impedance of a cell in an array, the contributions from the neighboring cells must also be included.

3.2.1 Mutual Radiation Impedance between Two cMUT Cells

If there are a number of transducers in the close proximity of the each other, one can define a mutual radiation impedance between them. The mutual radiation impedance, Z_{ij}, between ith and jth transducers is the power generated on the jth transducer due to the pressure generated by the ith transducer divided by the product of the reference velocities [72]

$$Z_{ij} = \frac{\int_{S_j} p_i(r_j) v_j^*(r_j) dS}{V_i V_j^*} \quad i, j = 1, 2 \ldots, \quad i \neq j \tag{3.10}$$

Using (3.3) with n=2 and 4, Z_{ij} is found as

$$Z_{ij} = \alpha_2^2 Z_{ij}^{22} + 2\alpha_2\alpha_4 Z_{ij}^{24} + \alpha_4^2 Z_{ij}^{44} \tag{3.11}$$

where Z_{ij}^{nm} is the mutual radiation impedance between the transducers having the velocity profiles $v_n(r)$ and $v_m(r)$ and it can be written as a double infinite

summation with μ and ν being the summation indices [69]

$$\begin{aligned} Z_{ij}^{nm} =& S\rho_0 c_0 \frac{2^{n+m} n! m! \sqrt{2n+1}\sqrt{2m+1}}{\sqrt{2kd_{ij}}(ka)^{n+m}} \\ & \times \sum_{\mu=0}^{\infty}\sum_{\nu=0}^{\infty} \left\{ \frac{\Gamma(\mu+\upsilon+1/2)}{\mu!\upsilon!} \left(\frac{a}{d_{ij}}\right)^{\mu+\upsilon} J_{\mu+n+1}(ka) J_{\upsilon+m+1}(ka) \right. \\ & \left. \times \left[J_{\mu+\upsilon+\frac{1}{2}}(kd_{ij}) + i(-1)^{\mu+\upsilon} J_{-\mu-\upsilon-\frac{1}{2}}(kd_{ij}) \right] \right\} \end{aligned} \tag{3.12}$$

where d_{ij} is the distance between ith and jth transducers.

3.2.2 Radiation Impedance of an Array of cMUT Cells

The calculation of the radiation impedance of an array of cMUT cells is demonstrated with an array, where equal size cells are placed in a hexagonal pattern giving the most compact arrangement [74]. Circular arrays as in Fig. 3.3 with N=7, 19, 37 and 61 cells are investigated. The center-to-center spacing between neighboring cells is d=2a to use the area in the most efficient way. The radiation

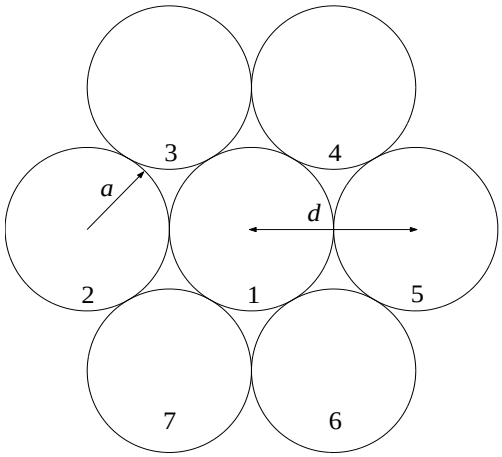

Figure 3.3: The geometry of a circular array with hexagonally placed N=7 cells and d=2a.

impedance of an N-cell array is modelled with an N-port linear network with a

symmetrical $N \times N$ Z-parameter matrix, where the diagonal elements are given by (3.9) and the off-diagonal elements are found from (3.12):

$$\begin{bmatrix} F_1 \\ F_2 \\ \vdots \\ F_N \end{bmatrix} = \begin{bmatrix} Z_{11} & Z_{12} & \dots & Z_{1N} \\ Z_{12} & Z_{11} & \dots & Z_{2N} \\ \vdots & \vdots & \ddots & \vdots \\ Z_{1N} & Z_{2N} & \dots & Z_{11} \end{bmatrix} \begin{bmatrix} V_1 \\ V_2 \\ \vdots \\ V_N \end{bmatrix} \tag{3.13}$$

Here, F_i is the force and V_i is the lumped rms velocity at the ith cell as shown in Fig. 3.4(a). The LC section models the mechanical impedance of the membrane, Z_m [45,55]. Due to the symmetry, the 7-port network of a 7-cell array in Fig. 3.3 can be simplified to

$$\begin{bmatrix} F_1 \\ F_2 \end{bmatrix} = [Z'] \begin{bmatrix} V_1 \\ 6V_2 \end{bmatrix} \tag{3.14}$$

where

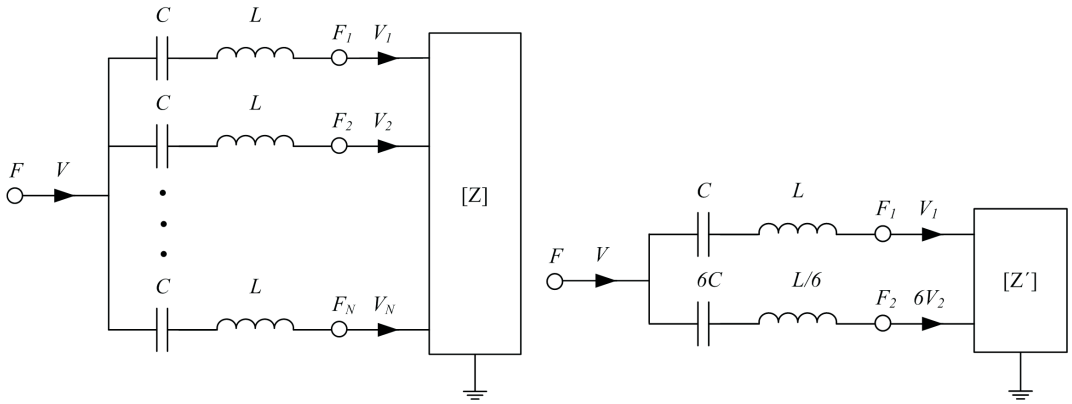

Figure 3.4: The equivalent circuit of the radiation impedance for (a) a general array and (b) a circular array with hexagonally placed N=7 cells.

$$[Z'] = \begin{bmatrix} Z_{11} & Z_{12} \\ Z_{12} & (Z_{11} + 2Z_{12} + 2Z_{24} + Z_{25})/6 \end{bmatrix} \tag{3.15}$$

since Z_{12}=Z_{23}=Z_{27} and Z_{24}=Z_{26}. The resulting equivalent circuit is depicted in Fig. 3.4(b). Since the radiation impedance of each cell is different, a representative radiation impedance, Z_r, of a single cell is defined as

$$Z_r = N\frac{F}{V} - Z_m = R_r + iX_r \tag{3.16}$$

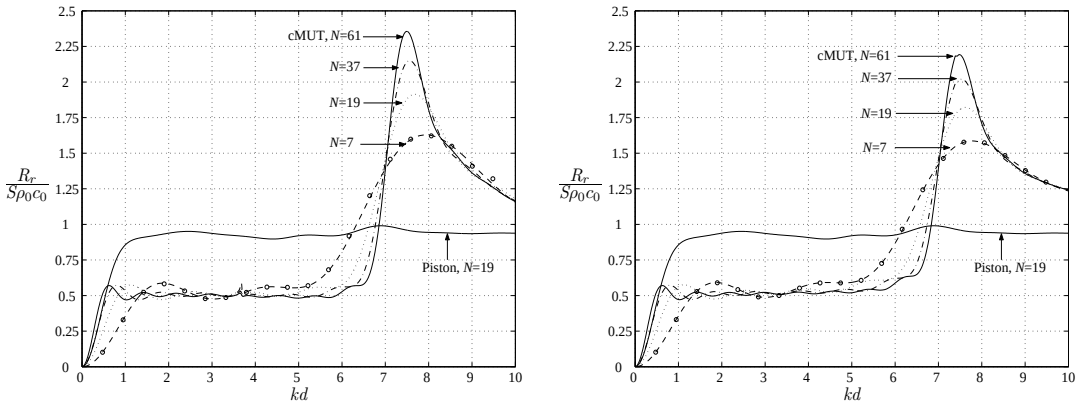

Figure 3.5: The representative radiation resistance, R_r, normalized by $S\rho_0 c_0$ of a single cMUT cell in N=7, 19, 37 and 61 element arrays in comparison to a cell in N=19 element piston array all with a/d=0.5 as a function of kd for a cMUT cell with (a) $k_p a$=2π and (b) $k_p a$=4π. The representative radiation resistance determined by FEM simulations (circles) are also shown.

where F and V are as shown in Fig. 3.4.

Fig. 3.5 shows the representative radiation resistance of a single cell normalized by $S\rho_0 c_0$ in various arrays as a function of kd for cMUT cells with $k_p a$=2π and 4π. For $kd < 5$, R_r of the cMUT cell shows a behavior similar to that of an array of pistons [62] except for the vertical scale. As kd increases, the positive loading on the each cell increases and R_r becomes maximum around kd=7.5, where the loading reaches an optimum point [73]. As N increases, the maximum value of the radiation resistance, R_{max} , also increases, while the corresponding kd value, kd_{opt}, is not significantly affected. On the other hand, as $kd \rightarrow \infty$, the mutual effects vanish and normalized value of R_r approaches to that of an individual cell. Note that for thin membranes with $k_p a < 3.7$, kd_{opt}=7.5 point is beyond the parallel resonance frequency, hence such a maximum will not be present.

The variation of R_{max} and kd_{opt} is investigated by changing the distance between the cells for an array with $k_p a$=4π. The first peak in the radiation resistance and the corresponding kd value are taken as R_{max} and kd_{opt}, respectively. As depicted in Fig. 3.6, a/d=0.42 and kd_{opt}=7.68 define the optimum separation for N=19. For example, at f=100 kHz, this maximum for an airborne cMUT

is reached when d=4.05 mm giving a=1.7 mm. If the cMUT cell is made of a silicon membrane, then its thickness needs to be 69 μm [61] to have a mechanical resonance at 100 kHz. As shown in Fig. 3.6, there is only a 3% improvement in the radiation resistance by making a/d=0.42 rather than the most compact arrangement of a/d=0.5. Although this sparse arrangement results in a reduction in the fill factor [74] of about 30%, it may be necessary anyway in fabricated arrays to leave space for anchors of the membrane. kd_{opt} varies between 7.5 and 8.3 and it is nearly independent of a/d as well as N.

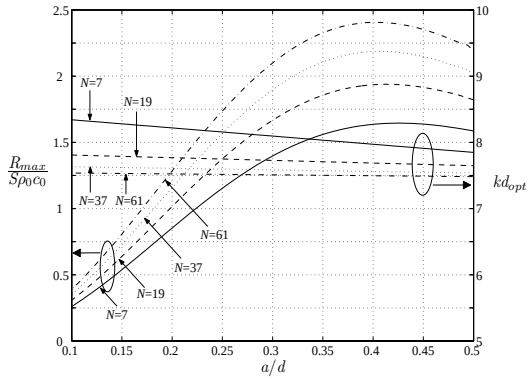

Figure 3.6: kd_{opt} and normalized R_{max} as a function of a/d for a cMUT cell with $k_p a$=4π in N=7, 19, 37 and 61 element arrays.

In this thesis, the radiation impedance is calculated for the radially symmetric velocity profiles. The cMUT membrane has an antisymmetric mode at $0.54 f_p$ between the series and the parallel resonance frequencies [75]. In a dense medium like water, this mode can be excited depending on the position of the cell in the array [62]. This is most pronounced for the array with N=7, since all the outer cells experience antisymmetric loading from the neighboring cells. To investigate this effect, the radiation impedance of an array made of cells with d=2.1a, $k_p a$=2.15 and 3.7 as determined by FEM simulations and calculated using (3.16) are shown in Fig. 3.7(a) [3]. For $k_p a$=2.15, it is seen that there is a dip in the radiation resistance near ka=0.54$k_p a$=1.16 (or kd=2.1 $\times$ 1.16=2.4) corresponding

[3]For both curves, there is a wiggle around $0.25 k_p a$ predicted by analytical approach as well as FEM simulations. This point corresponds to the series resonance frequency of the membrane. The wiggle is due to the parallel combination of series RLC circuits with slightly different resonance frequencies. It does not exist for high $k_p a$ values, since the quality factor of RLC circuits is lower.

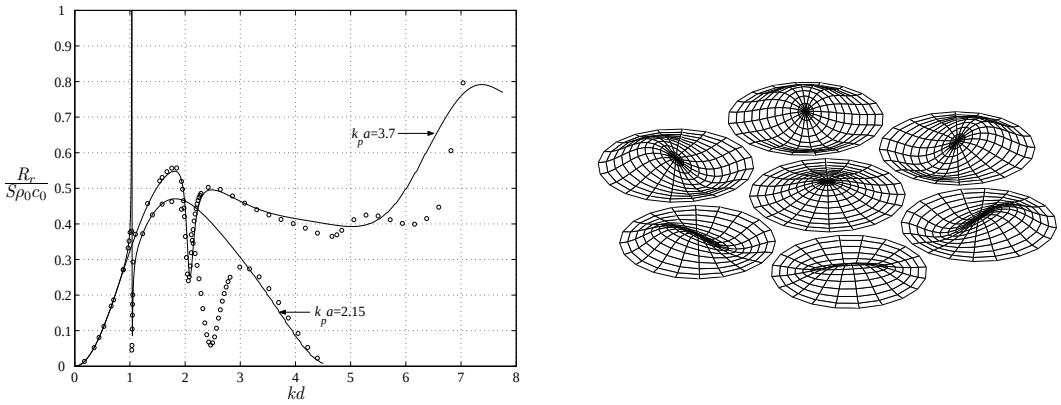

(a) (b)

Figure 3.7: (a) The representative radiation resistance normalized by $S\rho_0 c_0$ of a single cMUT cell in N=7 element array in water for a cell with d=2.1a, $k_p a$=2.15 and 3.7. The representative radiation resistance determined by FEM simulations (circles) are also depicted. Note that the $k_p a$=2.15 curve does not have the kd_{opt}=7.5 peak. The discrepancy between FEM simulations and analytic curve is due to the presence of antisymmetric mode. (b) FEM computed velocity profile of the cells showing the excitation of antisymmetric mode at the outer cells for $k_p a$=2.15 and kd=2.4.

to the antisymmetric mode as determined from FEM simulations, which is not predicted by (3.16). The velocity profiles of the cells showing the excitation of antisymmetric mode at this frequency can be seen in Fig. 3.7(b). As $k_p a$ increases, this effect is less pronounced. For $k_p a$=3.7, the dip is still present near kd=2.1 $\times$ 0.54$k_p a$=4.2, but it is smaller. As seen in Fig. 3.5, the dip is nonexistent in thicker membranes with $k_p a$=2π or $k_p a$=4π. Similarly, such dips are not present for airborne transducer arrays, since antisymmetric modes are not excited.

Chapter 4

AIRBORNE cMUTs

In this chapter, the performance of a cMUT array having a circular shape operating in air is optimized by increasing the radiation resistance of the array. This is achieved by choosing the size of the cMUT membranes and their placement within the array. The proposed approach improves the bandwidth as well as the transmitted power of the array. First, the radiation resistance of a cMUT array having a circular shape is optimized. Then, the quality factors of the various cMUT arrays are calculated. The transmit and the receive performances are calculated assuming the conventional operating conditions. The results are presented as normalized design graphs, which make them possible to be used for an arbitrary device dimensions and a material property. Design examples are given to demonstrate the use of these graphs.

4.1 Performance Figures

The cMUT cell operates around its series resonance frequency (f_r) in air [1,12,63]. In this section, a circular array, where the cells are placed in a hexagonal pattern, as depicted in Fig. 4.1 is investigated. The effective radius of the array, A, is equal to

$$A = a\sqrt{N/f_F} \quad \text{with} \quad f_F = (2\pi/\sqrt{3})(a/d)^2 \tag{4.1}$$

The effects of the parameters, a, A and d on the transmit and the receive performances of the cMUT are investigated while the other parameters are kept constant. A noise analysis is provided to determine the noise figure of the system including the receiver electronics. The membrane material is assumed to be silicon. Analytical expressions are presented for each performance figure. As a is changed, t_m and t_g are adjusted to keep the resonance frequency and the collapse voltage constant. In order to keep A constant at the specified value, N is adjusted as an integer variable. Since the acoustic loading is low,compared to the mechanical impedance of the membrane, the effect of the radiation reactance is ignored. The results are displayed on normalized graphs.

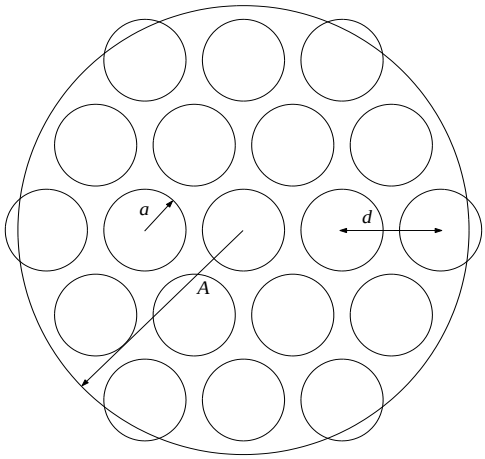

Figure 4.1: The geometry of a circular array with hexagonally placed N=19 cells.

4.1.1 Radiation Resistance

In the previous chapter, it is shown that the radiation resistance (R_r) of a cMUT cell in an array is a strong function of d [48]. It is maximized, when d is around $1.25\lambda_r$ for the most compact arrangement (d=2a). On the other hand, such an arrangement requires relatively large radius cells with relatively thick membranes to meet the resonance frequency requirement. However, a smaller cell radius would allow a thinner membrane with a potentially better bandwidth [63]. In

order to increase R_r for a smaller cell radius, d is made larger than $2a$ to get a sparse arrangement of the cells [64, 73, 76]. Fig. 4.2 shows the normalized radiation resistance (R_n) of a single cell in various arrays made of different cMUTs as a function of d/a and the variation of the optimum separation to maximize R_n, d_{opt}, and its value, R_{max}, with respect to a/λ_r.

As shown in Fig. 4.2(a), R_n can be maximized for a lower a value as d/a is increased [48, 64, 76]. At these points, the net loading on each cMUT is maximized [48, 64, 73, 76]. As A is increased, the maximum value of R_n for a given cMUT cell also increases. Note that for a membrane with a/λ_r=0.3 in an array with A/λ_r=3, R_n is more than three times higher when d/a=2.8 compared to the most compact arrangement of d/a=2.

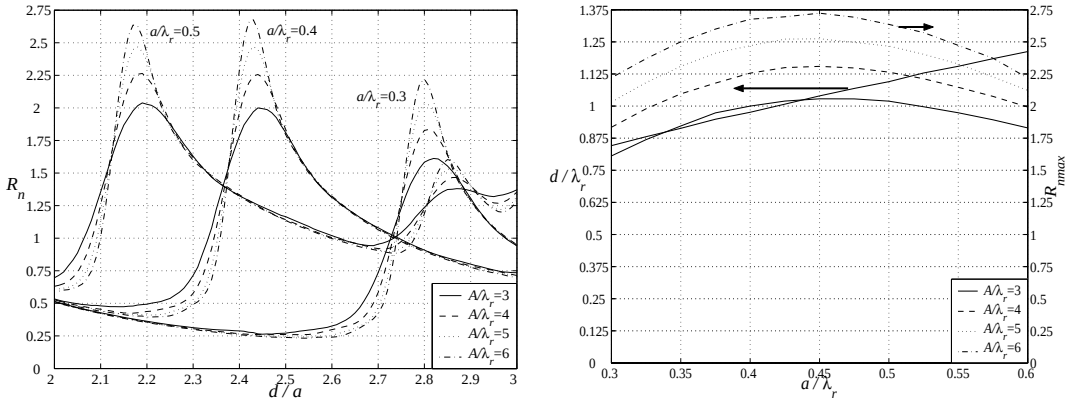

(a) (b)

Figure 4.2: (a) The normalized radiation resistance (R_n) of a single cell in various arrays as a function of d/a. (b) The change of the optimum separation (d_{opt}) and the maximum normalized radiation resistance (R_{max}) as a function of a/λ_r.

4.1.2 Q Factor

In air, Q is determined by the series RLC section at the mechanical side of the Mason's equivalent circuit [63]. Hence

$$Q = \frac{2\pi f_r L_m}{R_r} \tag{4.2}$$

Using (2.8) and (2.11) and expressing the membrane thickness (t_m) in terms of a and λ_r (2.10), Q (4.2) can be rewritten as

$$Q = \frac{23.8 c_0 \rho}{\rho_0} \sqrt{\frac{\rho(1-\nu^2)}{Y_0}} \frac{a^2}{\lambda_r^2 R_n} \tag{4.3}$$

As seen from (4.3), a smaller a is desirable since it reduces Q. On the other hand, a higher R_n also reduces Q by increasing the loading on the cell. Fig. 4.3 shows Q of various arrays made of different cMUTs as a function of d/a.

As depicted in Fig. 4.3, Q of each array has a minimum at the point, where R_n is maximized. For the most compact arrangement, Q for all devices are above 150, however with a sparse arrangement, it is possible to obtain Q below 50 without introducing any lossy elements to the system. For a fixed cell size, Q is lower when the cell is in a larger array due to increased R_n.

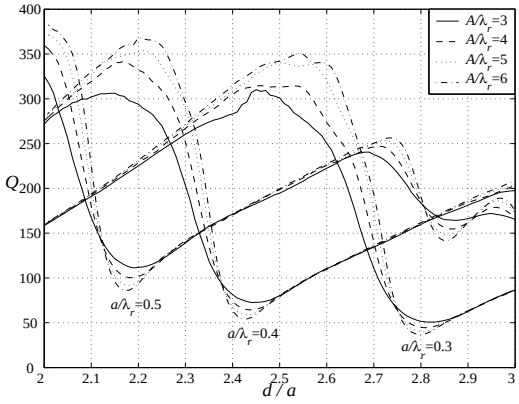

Figure 4.3: Q of various arrays as a function of d/a.

4.1.3 Transmit Mode

To maximize the power transferred to the medium, cMUT is driven such that the membrane swings the entire stable gap height (the allowed swing range of the membrane without collapsing), which is $0.46 t_g$ for the peak displacement [55]. The velocity of the membrane will be sinusoidal with frequency f_r, since Q is relatively high [77]. Then, rms velocity of the membrane is [55, 64, 76]

$$v_{rms} = \frac{2\pi f_r x_{rms}}{\sqrt{2}} = \frac{0.46\pi t_g f_r}{\sqrt{10}} \tag{4.4}$$

If t_g is expressed in terms of V_{col} from (2.6) and t_m is eliminated using (2.10), the average output power from a single cMUT cell is

$$P_{ave} = v_{rms}^2 R_r = \frac{0.045\rho_0 c_0}{\rho} \left(\frac{Y_0 \epsilon_0^2}{(1-\nu^2)} \right)^{1/3} a^{2/3} V_{col}^{4/3} R_n \tag{4.5}$$

and the average output power from the array will be N times of (4.5). Then

$$P_{ave} = N v_{rms}^2 R_r = \frac{0.16\rho_0 c_0}{\rho} \left(\frac{Y_0 \epsilon_0^2}{(1-\nu^2)} \right)^{1/3} \frac{a^{2/3} A^2 V_{col}^{4/3} R_n}{d^2} \tag{4.6}$$

Fig. 4.4 shows the average output power normalized by λ_r and V_{col} per unit area of various arrays made of different cMUTs as a function of d/a. It is seen that P_{ave} is maximized, when R_n is maximized (4.6). Note that as d/a increases, N decreases. Consequently for a/λ_r=0.3, P_{ave} is only 1.5 times higher, although the increase in R_n is more than 3 times compared to the most compact arrangement.

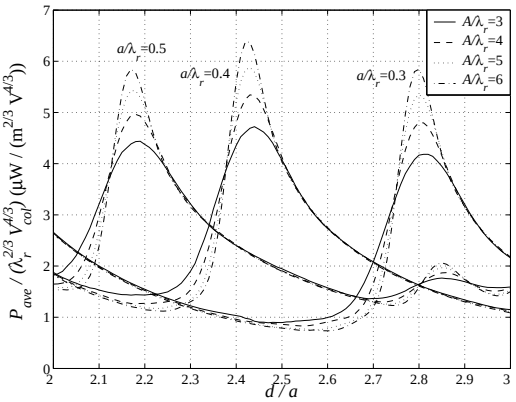

Figure 4.4: The average output power normalized by λ_r and V_{col} per unit area of various arrays as a function of d/a.

4.1.4 Receive Mode

The receive performance of a transducer is specified by its open-circuit voltage, V_{oc}, together with the input resistance, R_{in}, and the capacitance, C_{in}, hence the input impedance, Z_{in}, is given by the parallel combination of R_{in} and C_{in}. In order to calculate these parameters, C for C_{in} (2.5) and $\mathrm{d}C/\mathrm{d}x_{rms}$ for n hence

R_{in} (2.5, 2.7) are required. If a normalized displacement such that $x{=}x_{rms}/t_g$ is defined [78], then x will depend only on the ratio of the operating voltage to the collapse voltage (α) [55, 78]. Using (2.5), C and $\mathrm{d}C/\mathrm{d}x_{rms}$ are rewritten as

$$\begin{aligned} C &= \frac{\epsilon_0 \pi a^2}{t_g} \frac{\tanh^{-1}\left(\sqrt{\sqrt{5}x}\right)}{\sqrt{\sqrt{5}x}} \\ &= \frac{\epsilon_0 \pi a^2}{t_g} f_c(\alpha) \\ \frac{\mathrm{d}C}{\mathrm{d}x_{rms}} &= \frac{\epsilon_0 \pi a^2}{2t_g^2} \left(\frac{1}{x\left(1-\sqrt{5}x\right)} - \frac{\sqrt{\sqrt{5}x}}{x\sqrt{\sqrt{5}x}} \right) \\ &= \frac{\epsilon_0 \pi a^2}{2t_g^2} f_{\mathrm{d}C}(\alpha) \end{aligned} \tag{4.7}$$

The Mason's equivalent circuit in Fig. 2.6 is used to calculate the receive mode parameters. cMUT is excited by a force source with an amplitude of PS where P is the incident pressure field. α is assumed to be 0.9 giving f_c=1.11 and $f_{\mathrm{d}C}$=2.90. V_{oc} is given by the voltage division between the shunt input capacitance C and the remaining of the network. For the typical device dimensions and the operating frequencies in air, which is in the 1 mm and 100 kHz range, C shows a high impedance compared to the rest of the network and can be ignored. Then

$$\frac{V_{oc}}{P} = \frac{S}{n} = \frac{0.095 c_0^2}{\rho} \left(\frac{Y_0}{\epsilon_0(1-\nu^2)} \right)^{1/3} \frac{\lambda_r^2 V_{col}^{1/3}}{a^{4/3}} \tag{4.8}$$

which is independent of R_n. The material dependent part is equal to 1.2 $\times$ 10^8 (V $^{2/3}$ m$^{4/3}$)/N. The input resistance will be equal to the radiation resistance referred to the electrical side, whereas the input capacitance will be the shunt input capacitance. Then, R_{in} and C_{in} of a single cell are

$$\begin{aligned} R_{in} &= \frac{R_r}{n^2} = \frac{0.0029\rho_0}{c_0^3\rho^2} \left(\frac{Y_0^2}{\epsilon_0^2(1-\nu^2)^2} \right)^{1/3} \frac{\lambda_r^4 V_{col}^{2/3} R_n}{a^{14/3}} \\ C_{in} &= C = 1.22\rho_0\epsilon_0^{4/3} \left(\frac{Y_0}{\rho^3(1-\nu^2)} \right)^{1/6} \frac{a^{8/3}}{\lambda_r V_{col}^{2/3}} \end{aligned} \tag{4.9}$$

and since cMUTs in an array are connected in parallel, R_{in} and C_{in} of the array are

$$R_{in} = \frac{R_r}{Nn^2} = \frac{0.0008\rho_0}{c_0^3\rho^2}\left(\frac{Y_0^2}{\epsilon_0^2(1-\nu^2)^2}\right)^{1/3}\frac{d^2\lambda_r^4 V_{col}^{2/3} R_n}{a^{14/3}A^2}$$
$$C_{in} = NC = 4.45\rho_0\epsilon_0^{4/3}\left(\frac{Y_0}{\rho^3(1-\nu^2)}\right)^{1/6}\frac{a^{8/3}A^2}{d^2\lambda_r V_{col}^{2/3}} \tag{4.10}$$

Fig. 4.5 shows R_{in} and C_{in} normalized by λ_r and V_{col} per unit area of various arrays made of different cMUTs as a function of d/a. V_{oc} is independent of loading on the cells, hence d/a.

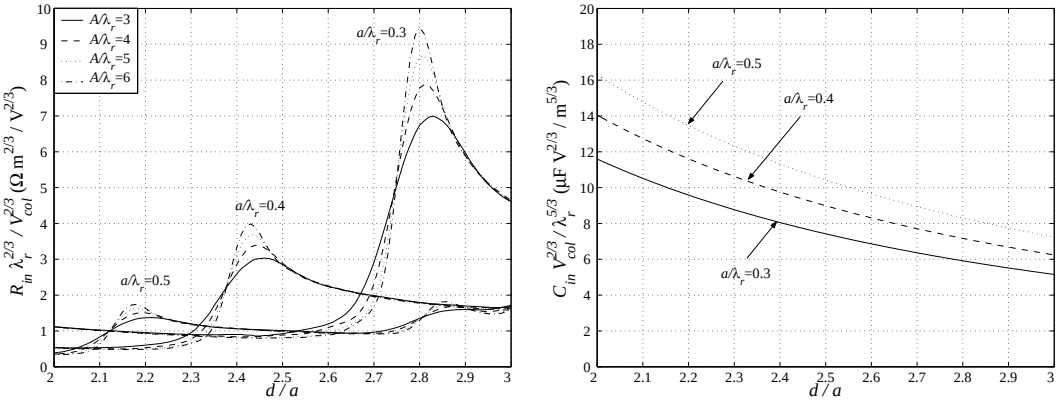

(a) (b)

Figure 4.5: (a) R_{in} (b) C_{in} normalized by λ_r and V_{col} per unit area of various arrays as a function of d/a.

4.1.5 Noise Analysis

An important figure of merit for the receive performance is the noise figure, F. In the receive circuitry, a very noise low noise OPAMP, MAXIM [1] MAX410 (BJT) and MAX4475 (FET), in both non-inverting and inverting configurations are used as shown in Fig. 4.6. The input referred noise voltage, e_n, and noise current, i_n, of this OPAMP are 1.2 nV/Hz$^{1/2}$ and 1.2 pA/Hz$^{1/2}$, respectively for MAX410, whereas 4.5 nV/Hz$^{1/2}$ and 0.5 fA/Hz$^{1/2}$ for MAX4475. The feedback resistors, R_1

[1] http://www.maxim.com

and R_2 are chosen as 1 kΩ and 10 kΩ. The noise contributions from the resistors can be decreased by connecting parallel capacitors, C_1 and C_2 with values of -100j and -1000j Ω at the operating frequency. Z_{opt} is determined from ANSOFT^{TM} simulations. For MAX410, Z_{opt} is 3.5 and 2.7 kΩ giving F of 2.55 and 3.86 dB for the non-inverting and the inverting configurations without the capacitors. With the capacitors, $Z_{opt} = R_{opt} + iX_{opt}$ is 1289 + j 90 and 524 + j 522 Ω giving F of 0.91 and 1.41 dB. For MAX4475, Z_{opt} is 11.8 M and 4.8 kΩ giving F of 0.0016 and 4.1 dB for the non-inverting and the inverting configurations without the capacitors. With the capacitors, $Z_{opt} = R_{opt} + iX_{opt}$ is 9M + j 409 and 4.3 + j 1.1 kΩ giving F of 0.0016 and 3.17 dB. Since the optimum source impedance to minimize the noise figure, Z_{opt}, is below a few kΩs, which is comparable to R_{in}, a BJT choice is preferable. Fig. 4.7 shows F of the receiver circuitries as the source resistance, R_s, is changed.

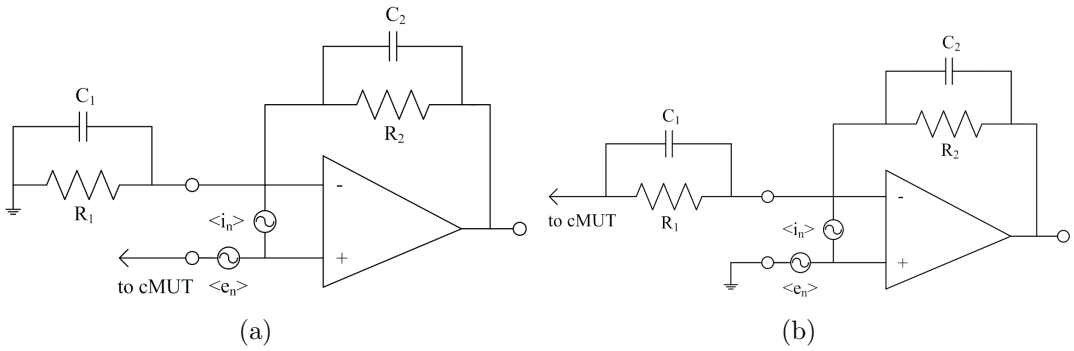

Figure 4.6: The receiver circuitry used in the calculations of the noise figure, OPAMP with (a) non-inverting (b) inverting configurations.

Minimizing the noise figure depends on the termination of the receiver amplifier with the optimum source resistance. Note that as the distance between the cells increases, due to the reduced fill factor, the intercepted input signal power decreases. This eventually decreases the noise figure. Table 4.1 shows the reduction in F with respect to d/a. Also if R_{in} of cMUT is lower compared to the real part of R_{opt}, it is possible to decrease F by clustering the cells [64], decreasing the number of the cells connected to the receiver amplifier.

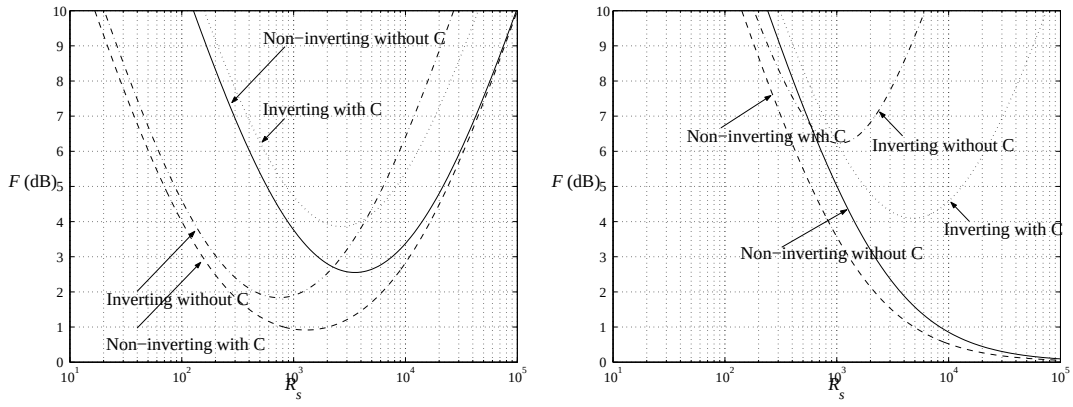

(a) (b)

Figure 4.7: F of various receiver circuitries as a function of R_s. (a) BJT (b) FET OPAMP

Table 4.1: Reduction in noise figure (dB).

d/a	2	2.1	2.2	2.3	2.4	2.5	2.6	2.7	2.8	2.9	3
F	0.41	0.81	1.25	1.6	2	2.3	2.68	3.01	3.28	3.57	3.87

4.2 Design Examples

Let's demonstrate the use of the normalized graphs with an example. Suppose that a cMUT array operating at 100 kHz (λ_r=3.3 mm) is required and the available area is 12.4 cm^2, equivalently A=19.9 mm=$6\lambda_r$. The radius of the single cell, a is chosen to be 0.99 mm=$0.3\lambda_r$ and corresponding t_m=23.5 μm from (2.10). Two designs are provided. In the first design, the choice of d/a=2 gives $N = (2\pi/\sqrt{3})(6^2/0.3^2 2^2)$=362 from (4.1). In the second design, d/a=2.8 is chosen and results in N=185. From Fig. 4.2(a), it is found that R_n=0.5 and 2.25 for d/a=2 and 2.8, respectively. Then, $R_r = \pi \times 0.99\text{mm}^2 \times 1.27 \times 331 \times 0.5$=647 kg/s for the former one from (2.11) and R_r=2900 kg/s for the latter one. This shows that cMUTs in the sparse array are better loaded by air.

Q factors of the designs can be determined from Fig. 4.3. For the first design (d/a=2), Q is equal to 160 giving a bandwidth of 625 Hz. For the second design (d/a=2.8), Q is equal to 45, with a bandwidth of 2.2 kHz.

Let the available bias voltage be 250 V, which is chosen to be V_{col} giving

t_g=7.2 μm from (2.6). From Fig. 4.4, the normalized output powers are read as 2.7 and 5.8 μW/(m$^{2/3}$V$^{4/3}$). Note that these values are for a unit circular area. Keeping in mind this, actual powers are $P_{ave} = 2.7\mu\text{W}\times3.3\text{mm}^{2/3} \times 250^{4/3} \times \pi \times 6^2$=10.7 mW and 23 mW for the first and the second designs, respectively. V_{oc} is calculated from (4.8) as 70 mV. Whereas, R_{in} is calculated as 17 and 150 Ω and C_{in} is 1.5 nF and 0.78 nF.

For the receiver circuitry, let's choose non-inverting amplifier with capacitors, which has the lowest noise figure. F is read as 4.9 and 3.04 dB, respectively. After the correction in Table 4.1 is made, F is 4.9 and 6.32 dB. Suppose that, there are four available receiver circuitries and each array is divided into four equal parts (clustering). Then, each part has an input resistance of 280 and 600 Ω. Then, F of each configuration will be 2.35 and 4.44 dB. Note that reduction in the fill factor severely degrades F.

Table 4.2: The comparison of the most compact and the sparse arrangements.

	N	R_r (kg/s)	Q	P_{ave} (mW)	V_{oc} (mV)	R_{in} (Ω)	C_{in} (nF)	F (dB)
d/a=2	362	647	160	10.7	70	17	1.5	4.9
d/a=2.8	185	2900	45	23	70	150	0.78	6.32

Chapter 5

CONCLUSION

Capacitive micromachined ultrasonic transducers (cMUTs) are competitive to the piezoelectric transducers due to the compatibility with silicon IC technology. They have a wider bandwidth with a lower transmit power and a receive sensitivity. But they are not on the medical imaging market, which seems to be the most profitable application area. In order to be commercialized, they should overcome these drawbacks, on which the active research is going on. An alternative way will be the use of cMUTs in areas, where the piezoelectric transducers perform poorly or cannot work. In this thesis, the latter approach is followed to design wide band and highly efficient airborne transducers with high output power.

In the first part, the radiation impedance of a cMUT with a circular clamped membrane is calculated up to its parallel resonance frequency. The velocity profile of the membrane is written as a superposition of analytic velocity profiles whose weights are dependent on frequency. These profiles are used to calculate the individual and the mutual radiation impedances from given expressions. Radiation impedance of any combination of cells can be found by considering only two cells at a time. Circular arrays are investigated to find the radiation resistances. It is found that the radiation resistance is a strong function of the separation of the cells. The center-to-center separation of the cells needs to be around 1.25λ (kd=7.8) for a high radiation resistance. Note that the optimum cell separation may require a cMUT cell with an unusually large radius. With an increased

radius, the thickness of the membrane must also be increased to preserve the resonance at the operating frequency. In this case, the gap height may have to be reduced to keep the bias voltage at an acceptable level, since an increased membrane thickness implies a higher bias voltage. The model is perfectly valid for airborne applications. However, for thin membranes with $k_p a < 4$, the model may fail in water immersion around the antisymmetric mode.

In the second part, the bandwidth of a cMUT array operating in air with a fixed area is optimized. The contradictory condition on the thickness of the membrane between the bandwidth and the output power is overcome by maximizing the radiation resistance with a proper choice of the cell size and the distance between the cells. It is shown that the thin membranes can have radiation resistances close to the maximum, which the thick membranes have. The Mason's equivalent circuit is used to measure cMUT performance. Analytical expressions are given for different operating modes. In order to make a fair comparison, the operating frequency and the collapse voltage of the devices are kept constant. The improvement in the bandwidth and the transmit power can be as high as three and one and a half times, respectively. The open circuit voltage is found to be independent of the radiation resistance. In order to calculate the noise figure of the system, a state of the art low noise OPAMP is used in the receiver circuitry. Two amplifier configurations are investigated. It is shown that noise figure close to the minimum noise figure of the receiver circuitry can be achieved by changing the number of the cells connected to the receiver, equivalently adjusting the input resistance. All results are presented as normalized design graphs, which are suited for the design of arbitrary size cMUTs.

The optimization process is suitable for the airborne applications, where the membrane impedance is much higher than the medium impedance. The increase in the bandwidth and the transmit power are proportional to the increase in the radiation resistance, since the bandwidth of the optimized radiation resistance is wider than the actual device bandwidth. On the other hand, in immersion applications, the membrane impedance is much lower than the medium impedance resulting in a wide bandwidth and this process is not suited except that the transducer will be only used for single frequency continuous wave excitation for high power transmission. It must be noted that since the acoustic impedance of the

immersion medium is high, the transmission process may result in the excitation of the antisymmetric modes in some cells of the array. This will be dominant especially in small symmetric shape arrays.

The future work for cMUTs must be to increase the transmit power and the sensitivity in order to compete with the piezoelectric transducers. One approach will be cMUTs to work at the collapse region with the optimized configuration [79], which seems to be the most promising way. The optimization includes the arrangement of the electrodes for the maximum transmit power and the receive voltage. It is possible to operate cMUTs beyond the maximum stable deflection point in conventional regime overcoming the collapse. There are several approaches used in MEMS devices also applicable to cMUTs. These are connecting a capacitor in series with the cMUT [80, 81], driving the cMUT with a current pulse [82] and use of a resonant drive [83, 84]. The leveraged bending approach [85] is already employed to cMUTs and very good results are obtained. This shows that the above methods will also increase the cMUT performance with a high probability.

Bibliography

[1] M. I. Haller and B. T. Khuri-Yakub, "A surface micromachined electrostatic ultrasonic air transducer," *IEEE Trans. Ultrason., Ferroelect., Freq. Contr.*, vol. 43, pp. 1–6, 1996.

[2] I. Ladabaum, X. Jin, H. T. Soh, A. Atalar, and B. T. Khuri-Yakub, "Surface micromachined capacitive ultrasonic transducers," *IEEE Trans. Ultrason., Ferroelect., Freq. Contr.*, vol. 45, pp. 678–690, 1998.

[3] X. Jin, I. Ladabaum, and B. T. Khuri-Yakub, "The microfabrication of capacitive ultrasonic transducers," *IEEE J. Microelectromech. Syst.*, vol. 7, pp. 295–302, 1998.

[4] Y. Huang, A. S. Ergun, E. Hæggström, M. H. Badi, and B. T. Khuri-Yakub, "Fabricating capacitive micromachined ultrasonic transducers with wafer-bonding technology," *IEEE J. Microelectromech. Syst.*, vol. 12, pp. 128–137, 2003.

[5] J. Knight, J. McLean, and F. L. Degertekin, "Low temperature fabrication of immersion capacitive micromachined ultrasonic transducers on silicon and dielectric substrates," *IEEE Trans. Ultrason., Ferroelect., Freq. Contr.*, vol. 51, pp. 1324–1333, 2004.

[6] A. S. Ergun, Y. Huang, X. Zhuang, Ö. Oralkan, G. G. Yaralıoğlu, and B. T. Khuri-Yakub, "Capacitive micromachined ultrasonic transducers: fabrication technology," *IEEE Trans. Ultrason., Ferroelect., Freq. Contr.*, vol. 52, pp. 2242–2258, 2005.

[7] J. Johnson, O. Oralkan, U. Demirci, S. Ergun, M. Karaman, and B. T. Khuri-Yakub, "Medical imaging using capacitive micromachined ultrasonic transducer arrays," *Ultrasonics*, vol. 40, pp. 471–476, 2002.

[8] F. L. Degertekin, M. Karaman, and R. O. Guldiken, "Forward-looking IVUS imaging using an annular-ring CMUT array," in *Proc. IEEE Ultrason. Symp.*, 2005, pp. 129–132.

[9] C. Daft, P. Wagner, B. Bymaster, S. Panda, K. Patel, and I. Ladabaum, "cMUTs and electronics for 2D and 3D imaging, monolithic integration, in-handle chip sets and system implications," in *Proc. IEEE Ultrason. Symp.*, 2005, pp. 463–474.

[10] G. Caliano, R. Carotenuto, E. Cianci, V. Foglietti, A. Caronti, A. Iual, and M. Pappalardo, "Design, fabrication and characterization of a capacitve micromachined ultrasonic probe for medical imaging," *IEEE Trans. Ultrason., Ferroelect., Freq. Contr.*, vol. 52, pp. 2259–2269, 2005.

[11] S. Olcum, M. N. Senlik, H. K. Oguz, A. Bozkurt, A. Atalar, and H. Köymen, "A wafer bonded capacitive micromachined underwater transducer," in *Proc. IEEE Ultrason. Symp.*, 2009, to be published.

[12] I. O. Wygant, M. Kupnik, J. C. Windsor, W. M. Wright, M. S. Wochner, G. G. Yaralioglu, M. F. Hamilton, and B. T. Khuri-Yakub, "50 kHz capacitive micromachined ultrasonic transducers for generation of highly directional sound with parametric arrays," *IEEE Trans. Ultrason., Ferroelect., Freq. Contr.*, vol. 56, pp. 193–203, 2009.

[13] S. T. Hansen, A. S. Ergun, W. Liou, B. A. Auld, and B. T. Khuri-Yakub, "Wideband micromachined capacitive microphones with radio frequency detection," *J. Acoust. Soc. Am.*, vol. 116, pp. 828–842, 2004.

[14] N. A. Hall, B. Bicen, M. K. Jeelani, W. Lee, S. Qureshi, and F. L. Degertekin, "Micromachined microphones with diffraction-based optical displacement detection," *J. Acoust. Soc. Am.*, vol. 118, pp. 3000–3009, 2005.

[15] I. Ladabaum, X. C. Jin, and B. T. Khuri-Yakub, "Air coupled through transmission of aluminum and other recent results using MUTs," in *Proc. IEEE Ultrason. Symp.*, 1997, pp. 983–986.

[16] I. J. Oppenheim, A. Jain, and D. W. Greve, "MEMS ultrasonic transducers for the testing of solids," *IEEE Trans. Ultrason., Ferroelect., Freq. Contr.*, vol. 50, pp. 305–311, 2003.

[17] J. McLean and F. L. Degertekin, "Capacitive micromachined ultrasonic transducers with asymmetric membranes for microfluidic applications," in *Proc. IEEE Ultrason. Symp.*, 2001, pp. 925–928.

[18] ——, "Interdigital capacitive micromachined ultrasonic transducers for microfluidic applications," in *Proc. IEEE Ultrason. Symp.*, 2003, pp. 1171–1174.

[19] G. G. Yaralioglu, M. H. Badi, A. S. Ergun, C. H. Cheng, B. T. Khuri-Yakub, and F. L. Degertekin, "Lamb wave devices using capacitive micromachined ultrasonic transducers," *Appl. Phys. Lett.*, vol. 78, pp. 111–113, 2001.

[20] J. McLean and F. L. Degertekin, "Directional scholte wave generation and detection using interdigital capacitive micromachined ultrasonic transducers," *IEEE Trans. Ultrason., Ferroelect., Freq. Contr.*, vol. 51, pp. 756–764, 2004.

[21] F. L. Degertekin, A. G. Onaran, M. Balantekin, W. Lee, N. A. Hall, and C. F. Quate, "Sensor for direct measurement of interaction forces in probe microscopy," *Appl. Phys. Lett.*, vol. 87, 2005.

[22] A. G. Onaran, M. Balantekin, W. Lee, W. L. Hughes, B. A. Buchine, R. O. Guldiken, Z. Parlak, C. F. Quate, and F. L. Degertekin, "A new atomic force microscope probe with force sensing integrated readout and active tip," *Review of Scientific Instruments*, vol. 77, pp. 023 501–1, 023 501–7, 2006.

[23] K. K. Park, H. J. Lee, G. G. Yaralioglu, A. S. Ergun, O. Oralkan, M. Kupnik, C. F. Quate, B. T. Khuri-Yakub, T. Braun, J.-P. Ramseyer, H. P. Lang, M. Hegner, C. Gerber, and J. K. Gimzewski, "Capacitive micromachined

ultrasonic transducers for chemical detection in nitrogen," *Appl. Phys. Lett.*, vol. 91, pp. 094 102–1, 094 102–3, 2007.

[24] J.-P. Raskin, A. R. Brown, B. T. Khuri-Yakub, and G. M. Rebeiz, "A novel parametric-effect MEMS aplifier," *IEEE J. Microelectromech. Syst.*, vol. 9, pp. 528–537, 2000.

[25] D. W. Greve, A. Jain, and I. J. Oppenheim, "MEMS phased array detection in contact with solids," in *Proc. IEEE Ultrason. Symp.*, 2002, pp. 1035–1038.

[26] A. Octavio, C. J. Martín, Y. Gómez-Ullate, O. Martínez, L. Gómez-Ullate, F. M. de Espinosa, P. Gatta, and M. Domínguez, "Design and characterization of air coupled ultrasonic transducers based on MUMPs," in *Proc. IEEE Ultrason. Symp.*, 2006, pp. 2373–2376.

[27] J. Liu, C. Oakley, and R. Shandas, "Capacitive micromachined ultrasonic transducers using commercial multi-user MUMPs process: capability and limitations," *Ultrasonics*, vol. 49, pp. 765–773, 2009.

[28] D. M. Mills and L. S. Smith, "Real-time in-vivo imaging with capacitive micromachined ultrasonic transducers (CMUT) linear arrays," in *Proc. IEEE Ultrason. Symp.*, 2003, pp. 568–571.

[29] D. M. Mills, "Medical imaging with capacitive micromachined ultrasonic transducers," in *Proc. IEEE Ultrason. Symp.*, 2004, pp. 384–390.

[30] J. G. Knight and F. L. Degertekin, "Capacitive micromachined ultrasonic transducers for forward looking intravascular imaging arrays," in *Proc. IEEE Ultrason. Symp.*, 2002, pp. 1079–1082.

[31] Y. Huang, E. O. Hæggström, X. Zhuang, A. S. Ergun, and B. T. Khuri-Yakub, "Optimized membrane configuration improves CMUT performance," in *Proc. IEEE Ultrason. Symp.*, 2004, pp. 505–508.

[32] ——, "Capacitive micromachined ultrasonic transducers CMUTs with piston-shaped membranes," in *Proc. IEEE Ultrason. Symp.*, 2005, pp. 589–592.

[33] M. N. Senlik, S. Olcum, and A. Atalar, "Improved performance of cMUT with nonuniform membranes," in *Proc. IEEE Ultrason. Symp.*, 2005, pp. 597–600.

[34] D. W. Greve and I. J. Oppenheim, "Theory of a double-diaphragm MEMS ultrasonic transducer," in *Proc. IEEE Ultrason. Symp.*, 2003, pp. 473–476.

[35] M. Pappalardo, G. Caliano, A. Caronti, and F. D. Alessio, "Capacitive ultrasonic transducers with a new vibrating structure," in *Proc. IEEE Ultrason. Symp.*, 2003, pp. 1955–1959.

[36] B. Bayram, E. Hæggström, G. G. Yaralioglu, and B. T. Khuri-Yakub, "A new regime for operating capacitive micromachined ultrasonic transducers," *IEEE Trans. Ultrason., Ferroelect., Freq. Contr.*, vol. 50, pp. 1184–1190, 2003.

[37] A. S. Ergun, B. Temelkuran, E. Ozbay, and A. Atalar, "A new detection method for capacitive micromachined ultrasonic transducers," *IEEE Trans. Ultrason., Ferroelect., Freq. Contr.*, vol. 48, pp. 932–942, 2001.

[38] N. A. Hall and F. L. Degertekin, "Integrated optical interferometric detection method for micromachined capacitive acoustic transducers," *Appl. Phys. Lett.*, vol. 80, pp. 3859–3861, 2002.

[39] S. Olcum, M. N. Senlik, and A. Atalar, "Optimization of the gain-bandwidth product of capacitive micromachined ultrasonic transducers," *IEEE Trans. Ultrason., Ferroelect., Freq. Contr.*, vol. 52, pp. 2211–2219, 2005.

[40] S. Peng, M. S. Qureshi, A. Basu, R. O. Guldiken, F. L. Degertekin, and P. E. Hasler, "Floating-gate based CMUT sensing circuit using capacitive feedback charge amplifier," in *Proc. IEEE Ultrason. Symp.*, 2006, pp. 2425–2428.

[41] W. P. Mason, *Electromechanical transducers and wave filters*, 2nd ed. New York: D. Van Nostrand Company, Inc., 1948.

[42] A. Caronti, R. Carotenuto, and M. Pappalardo, "Electromechanical coupling factor of capacitive micromachined ultrasonic transducers," *J. Acoust. Soc. Am.*, vol. 113, pp. 279–288, 2003.

[43] S. Olcum, A. Atalar, H. Köymen, and M. N. Senlik, "Calculation of transformer ratio in mason's equivalent circuit for cMUTs," in *Proc. IEEE Ultrason. Symp.*, 2006, pp. 1947–1950.

[44] A. Ronnekleiv, I. Ladabaum, X. C. Jin, and B. T. Khuri-Yakub, "An improved circuit model of MUTs," in *Proc. IEEE Ultrason. Symp.*, 1997, pp. 395–399.

[45] H. Köymen, M. N. Şenlik, A. Atalar, and S. Olcum, "Parametric linear modeling of circular cMUT membranes in vacuum," *IEEE Trans. Ultrason., Ferroelect., Freq. Contr.*, vol. 54, pp. 1229–1239, 2007.

[46] G. G. Yaralioglu, M. H. Badi, A. S. Ergun, and B. T. Khuri-Yakub, "Improved equivalent circuit and finite element method modeling of capacitive micromachined ultrasonic transducers," in *Proc. IEEE Ultrason. Symp.*, 2003, pp. 469–472.

[47] A. Rønnekleiv, "CMUT array modeling through free acoustic CMUT modes and analysis of the fluid CMUT interface through fourier transform methods," *IEEE Trans. Ultrason., Ferroelect., Freq. Contr.*, vol. 52, pp. 2173–2184, 2005.

[48] M. N. Senlik, S. Olcum, H. Köymen, and A. Atalar, "Radiation impedance of an array of circular capacitive micromachined ultrasonic transducers," *IEEE Trans. Ultrason., Ferroelect., Freq. Contr.*, accepted for publication.

[49] A. Bozkurt, I. Ladabaum, A. Atalar, and B. T. Khuri-Yakub, "Theory and analysis of electrode size optimization for capacitive microfabricated ultrasonic transducers," *IEEE Trans. Ultrason., Ferroelect., Freq. Contr.*, vol. 46, pp. 1364–1374, 1999.

[50] Y. Roh and B. T. Khuri-Yakub, "Finite element modeling of capacitor micromachined ultrasonic transducers," in *Proc. IEEE Ultrason. Symp.*, 2000, pp. 905–908.

[51] G. G. Yaralioglu, A. S. Ergun, and B. T. Khuri-Yakub, "Finite-element analysis of capacitive micromachined ultrasonic transducers," *IEEE Trans. Ultrason., Ferroelect., Freq. Contr.*, vol. 52, pp. 2185–2198, 2005.

[52] D. Certon, F. Teston, and F. Patat, "A finite difference model for cMUT devices," *IEEE Trans. Ultrason., Ferroelect., Freq. Contr.*, vol. 52, pp. 2199–2210, 2005.

[53] G. Caliano, A. Caronti, M. Baruzzi, A. Rubini, A. Iula, R. Carotenuto, and M. Pappalardo, "Pspice modeling of capacitive microfabricated ultrasonic transducers," *Ultrasonics*, vol. 40, pp. 449–455, 2002.

[54] H. K. Oguz, S. Olcum, M. N. Şenlik, V. Taş, A. Atalar, and H. Köymen, "Nonlinear modelling of an immersed transmitting capacitive micromachined ultrasonic transducer for harmonic balance analysis," *IEEE Trans. Ultrason., Ferroelect., Freq. Contr.*, accepted for publication.

[55] I. O. Wygant, M. Kupnik, and B. T. Khuri-Yakub, "Analytically calculating membrane displacement and the equivalent circuit model of a circular cMUT cell," in *Proc. IEEE Ultrason. Symp.*, 2008, pp. 2111–2114.

[56] E. C. Wente, "A condenser transmitter as a uniformly sensitive instrument for the absolute measurement of sound intensity," *Phys. Rev.*, vol. 10, pp. 39–63, 1917.

[57] D. Stansfield, *Underwater electroacoustic transducers.* Bath: Bath University Press and Institute of Acoustics, 1991.

[58] A. Lohfink, P.-C. Eccardt, W. Benecke, and H. Meixner, "Derivation of a 1D cMUT model from FEM results for linear and nonlinear equivalent circuit simulation," in *Proc. IEEE Ultrason. Symp.*, 2003, pp. 465–468.

[59] A. Bozkurt and M. Karaman, "A lumped circuit model for the radiation impedance of a 2D cMUT array element," in *Proc. IEEE Ultrason. Symp.*, 2005, pp. 1929–1932.

[60] F. Y. Yamaner and A. Bozkurt, "A lumped circuit model for the mutual radiation impedance of acoustic array elements," in *Proc. IEEE Ultrason. Symp.*, 2006, pp. 2385–2388.

[61] M. N. Senlik, A. Atalar, H. Koymen, and S. Olcum, "Radiation impedance and equivalent circuit for immersed CMUT array element," in *Proc. IEEE Ultrason. Symp.*, 2006, pp. 1951–1954.

[62] A. Caronti, A. Savoia, G. Caliano, and M. Pappalardo, "Acoustic coupling in capacitive microfabricated ultrasonic transducers: modeling and experiments," *IEEE Trans. Ultrason., Ferroelect., Freq. Contr.*, vol. 52, pp. 2220–2234, 2005.

[63] S. Olcum, A. Atalar, H. Köymen, and M. N. Senlik, "Stagger tuned cMUT array for wideband airborne applications," in *Proc. IEEE Ultrason. Symp.*, 2006, pp. 2377–2380.

[64] M. N. Senlik, S. Olcum, H. Köymen, and A. Atalar, "Bandwidth, power and noise considerations in airborne cMUTs," in *Proc. IEEE Ultrason. Symp.*, 2009, to be published.

[65] S. D. Senturia, *Microsystem design.* New York: Springer, 2000.

[66] M. Kupnik, I. O. Wygant, and B. T. Khuri-Yakub, "Finite element analysis of stress stiffening effects in CMUTs," in *Proc. IEEE Ultrason. Symp.*, 2008, pp. 487–490.

[67] Y. Nemirovsky and O. Bochobza-Degani, "A methodology and model for the pull-in parameters of electrostatic actuators," *IEEE J. Microelectromech. Syst.*, vol. 10, pp. 601–615, 2001.

[68] D. T. Blackstock, *Fundamentals of physical acoustics.* New York: John Wiley & Sons, Inc., 2000.

[69] D. T. Porter, "Self- and mutual-radiation impedance and beam patterns for flexural disks in a rigid plane," *J. Acoust. Soc. Am.*, vol. 36, pp. 1154–1161, 1964.

[70] M. Greenspan, "Piston radiator: some extensions of the theory," *J. Acoust. Soc. Am.*, vol. 65, pp. 608–621, 1979.

[71] L. L. Foldy, "Theory of passive linear electroacoustic transducers with fixed velocity distribution," *J. Acoust. Soc. Am.*, vol. 21, pp. 595–604, 1949.

[72] C. H. Sherman, "Analysis of acoustic interactions in transducer arrays," *IEEE Trans. Sonics Ultrason.*, vol. 13, pp. 9–15, 1966.

[73] H. Lee, J. Tak, W. Moon, and G. Lim, "Effects of mutual impedance on the radiation characteristics of transducer arrays," *J. Acoust. Soc. Am.*, vol. 115, pp. 666–679, 2004.

[74] R. L. Pritchard, "Mutual acoustic impedance between radiators in an infinite rigid plane," *J. Acoust. Soc. Am.*, vol. 32, pp. 730–737, 1960.

[75] A. Leissa, *Vibration of shells*. Washington D.C.: NASA, 1973.

[76] N. Portman-Senlik, "Analysis and design of capacitive micromachined ultrasonic transducers for airborne applications," *IEEE Trans. Ultrason., Ferroelect., Freq. Contr.*, in preparation.

[77] R. C. Dorf and R. H. Bishop, *Modern control systems*, 10th ed. New Jersey: Prentice Hall, 2004.

[78] L. M. Castañer and S. D. Senturia, "Speed-energy optimization of electrostatic actuators based on pull-in," *IEEE J. Microelectromech. Syst.*, vol. 8, pp. 290–298, 1999.

[79] S. Olcum, private communication, 2010.

[80] J. I. Seeger and S. B. Crary, "Stabilization of electrostatically actuated mechanical devices," in *Transducers '97*, 1997, pp. 1133–1136.

[81] E. K. Chan and W. Dutton, "Electrostatic micromechanical actuator with extended range of travel," *IEEE J. Microelectromech. Syst.*, vol. 9, pp. 321–328, 2000.

[82] L. M. Castañer, J. Pons, R. Nadal-Guardia, and A. Rodríguez, "Analysis of the extended operation range of electrostatic actuators by current-pulse drive," *Sens. Actuators A*, vol. 90, pp. 181–190, 2001.

[83] J. M. Kyynäräinen, A. S. Oja, and H. Seppä, "Increasing the dynamic range of a micromechanical moving-plate capacitor," *Analog Integrated Circuits and Signal Processing*, vol. 29, pp. 61–70, 2001.

[84] B. Cagdaser and B. E. Boser, "Resonant drive for stabilizing parallel-plate actuators beyond the pull-in point," in *Transducers '05*, 2005, pp. 688–692.

[85] E. S. Hung and S. D. Senturia, "Extending the travel range of analog-tuned electrostatic actuators," *IEEE J. Microelectromech. Syst.*, vol. 8, pp. 497–505, 1999.